Kinetic or thermal AGN feedback in simulations of isolated and merging disc galaxies calibrated by the $M-\sigma$ relation

Paramita Barai,[1][*] Matteo Viel,[1,2] Giuseppe Murante,[1] Massimo Gaspari[3] and Stefano Borgani[1,2,4]

[1]*INAF – Osservatorio Astronomico di Trieste, Via G.B. Tiepolo 11, I-34143 Trieste, Italy*
[2]*INFN/National Institute for Nuclear Physics, Via Valerio 2, I-34127 Trieste, Italy*
[3]*Max Planck Institute for Astrophysics, Karl-Schwarzschild-Strasse 1, D-85741 Garching, Germany*
[4]*Dipartimento di Fisica dell'Università di Trieste, Sezione di Astronomia, Via Tiepolo 11, I-34131 Trieste, Italy*

ABSTRACT

We investigate two modes of coupling the feedback energy from a central active galactic nucleus (AGN) to the neighbouring gas in galaxy simulations: *kinetic* – velocity boost and *thermal* – heating. We formulate kinetic feedback models for energy-driven wind (EDW) and momentum-driven wind (MDW), using two free parameters: feedback efficiency ϵ_f and AGN wind velocity v_w. A novel numerical algorithm is implemented in the smoothed particle hydrodynamics code GADGET-3, to prevent the expansion of a hole in the gas distribution around the black hole (BH). We perform simulations of isolated evolution and merger of disc galaxies, of Milky Way mass as well as lower and higher masses. We find that in the isolated galaxy BH kinetic feedback generates intermittent bipolar jet-like gas outflows. We infer that current prescriptions for BH subgrid physics in galaxy simulations can grow the BH to observed values even in an isolated disc galaxy. The BH growth is enhanced in a galaxy merger, which consequently requires different model parameters to fit the observations than an isolated case. Comparing the $[M_{BH}-\sigma_\star]$ relation obtained in our simulations with observational data, we conclude that it is possible to find parameter sets for a fit in all the models (e.g. $v_w = 10\,000\,\mathrm{km\,s^{-1}}$ and $\epsilon_f = 0.25$ for BH kinetic EDW), except for the case with MDW feedback in a galaxy merger, in which the BH is always too massive. The BH thermal feedback implementation of Springel et al. within the multiphase star formation model is found to have negligible impact on gas properties, and the effect claimed in all previous studies is attributed to gas depletion around the BH by the creation of an artificial hole. The BH mass accretion rate in our simulations exhibit heavy fluctuations. The star formation rate is quenched with feedback by removal of gas. The circumgalactic medium gas at galactocentric distances $(20–100)\,h^{-1}$ kpc is found to give the best metallicity observational diagnostic to distinguish between BH models.

Key words: black hole physics – methods: numerical – galaxies: active – galaxies: evolution – galaxies: interactions – cosmology: theory.

1 INTRODUCTION

Supermassive black holes (SMBHs) are believed to exist at the centres of active galaxies (e.g. Kormendy & Richstone 1995; Ferrarese & Ford 2005), powered by the accretion of matter and liberating enormous amounts of energy. Active galactic nuclei (AGN) influence the formation and evolution of galaxies in the form of feedback

(e.g. Silk & Rees 1998; King 2003; Granato et al. 2004; Begelman & Nath 2005; Barai & Wiita 2006; Croton et al. 2006; Barai 2008; Fabian 2012; Wagner, Umemura & Bicknell 2013), generating observational trends such as the central SMBH – host galaxy stellar bulge correlations (e.g. Magorrian et al. 1998; Gebhardt et al. 2000; Shankar et al. 2006). The energy output is often observed as AGN outflows in a wide variety of forms (see Crenshaw, Kraemer & George 2003; Everett 2007 for reviews), e.g. collimated relativistic jets and/or huge overpressured cocoons in radio (Nesvadba et al. 2008), blueshifted broad absorption lines in the UV and optical

[*]E-mail: pbarai@oats.inaf.it

(Reichard et al. 2003; Rupke & Veilleux 2011), warm absorbers (Krongold et al. 2007) and ultrafast outflows (Tombesi et al. 2013) in X-rays, molecular gas in far-IR (Feruglio et al. 2010; Sturm et al. 2011).

Concordance galaxy formation models in the cold dark matter (DM) cosmology widely incorporate feedback from AGN in simulations of isolated galaxies and mergers (e.g. Springel, Di Matteo & Hernquist 2005; Johansson, Burkert & Naab 2009b), and cosmological volumes (e.g. Sijacki et al. 2007; Booth & Schaye 2009; Dubois et al. 2010; Fabjan et al. 2010; Barai, Martel & Germain 2011b; Di Matteo et al. 2012; Hirschmann et al. 2013) as well as semi-analytical studies (e.g. Salucci et al. 1999; Shankar et al. 2004). Simulations generally invoke AGN feedback in the negative form which quenches star formation (SF) and limits the formation of massive stellar systems (e.g. Scannapieco, Silk & Bouwens 2005; van de Voort et al. 2011; Dubois et al. 2013b), as supported by some observations (e.g. Schawinski et al. 2006; Wang et al. 2007). At the same time, AGN feedback can be positive occasionally which also plays an important role in the cosmological context. AGN outflows have been shown to overpressure, compress and fragment clumpy gas clouds, triggering starbursts, in theoretical and numerical studies (e.g. De Young 1989; Silk 2005; Zubovas et al. 2013), and observed in jet-induced SF and radio–optical alignment (e.g. Chambers, Miley & van Breugel 1987; Zinn et al. 2013).

We investigate, in this paper, different models and implementation of AGN feedback in galaxy simulations. Our goal is to compare and contrast two modes of coupling of the feedback energy from black hole (BH) to the surrounding gas: *thermal* – where the gas temperature (or, internal energy) is increased and *kinetic* – where the gas velocity is boosted. We aim to find the model parameters in each case which fits relevant observational data, and explore the signatures of various feedback models on the BH growth, galaxy and circumgalactic medium (CGM) properties. In this work, we perform simulations of isolated and merging disc galaxies, before applying our models to cosmological volumes in the future.

Galaxy formation simulations have investigated both AGN feedback mechanisms: thermal (e.g. Di Matteo, Springel & Hernquist 2005; Sijacki et al. 2007; Booth & Schaye 2009; Fabjan et al. 2010; Gaspari et al. 2011b) and kinetic (e.g. Germain, Barai & Martel 2009; Dubois et al. 2010; Ostriker et al. 2010; Gaspari, Brighenti & Temi 2012a; Vazza, Bruggen & Gheller 2013). Gaspari et al. (2011a) explored several feedback mechanisms in galaxy clusters, including cold gas accretion and massive subrelativistic outflows, that self-regulate the mechanical power from AGN outflow heating. These models were extended by Gaspari et al. (2011b) to galaxy groups. Gaspari et al. (2012a) studied the role of mechanical AGN feedback in controlling the thermodynamical evolution of isolated elliptical galaxies. Gaspari, Ruszkowski & Sharma (2012b) explored the formation of multiphase gas via thermal instability in cluster cores heated by collimated bipolar AGN jets.

There have been two contemporary studies of BH feedback in isolated galaxy systems, the distinction of our work from those is outlined below. Newton & Kay (2013) simulated isolated and merging disc galaxies to investigate the effect of feedback from both AGN and supernovae (SNe) on galaxy evolution, and to isolate the most important factors of these feedback processes. They utilize different methods for distributing the feedback energy in the same thermal form, and do not have kinetic feedback. Our work considers the kinetic mode in addition to thermal.

Wurster & Thacker (2013b) compared the AGN feedback algorithms of four authors (Springel et al. 2005; Okamoto, Nemmen & Bower 2008; Booth & Schaye 2009; Debuhr, Quataert & Ma

2011) together with their own model in galaxy merger simulations, and found wide variation in accretion behaviours. Among these, in Debuhr et al. (2011) the feedback is returned as momentum or in the kinetic form, while the others have thermal feedback. However, the model by Debuhr et al. (2011) also has a distinct accretion prescription based on the viscous transport of angular momentum; therefore, comparing it with e.g. Springel et al. (2005, which uses the modified Bondi accretion rate) makes it hard to disentangle if the differential effects are because of various accretion methods or varying feedback models. In our study, we use the same accretion methodology and then compare between thermal versus kinetic modes of feedback.

This paper is organized as follows: we describe our numerical code and simulation setup in Section 2, in Section 3 we present and analyse our results, some important outcomes are discussed in Section 4, while in Section 5 we give a summary of the main findings and discuss possible future applications.

2 NUMERICAL METHOD

We use a modified version of the TreePM (particle mesh) – smoothed particle hydrodynamics (SPH) code GADGET-3 (Springel 2005), which includes a more efficient domain decomposition to improve the work-load balance over the public version GADGET-2. Some of the subgrid[1] physics included in the semipublic version of GADGET-3 code we use are outlined below. The BH modules including our new kinetic feedback model are described in Sections 2.1, 2.2 and 2.3. The initial galaxy models are presented in Section 2.4, and our simulations are mentioned in Section 2.5.

The non-AGN subgrid models: radiative physics, SF and chemical evolution are same as in the work of Barai et al. (2013). Radiative cooling and heating is computed by adding metal-line cooling from Wiersma, Schaye & Smith (2009), considering 11 different elements: H, He, C, Ca, O, N, Ne, Mg, S, Si and Fe. A photoionizing background radiation from the cosmic microwave background and the Haardt & Madau (2001) model for the UV/X-ray background are considered.

SF is implemented following the multiphase effective subresolution model by Springel & Hernquist (2003). Gas particles with density above a limiting threshold, $\rho_{SF} = 0.13\,\mathrm{cm}^{-3}$ (units of number density of hydrogen atoms), contain cold and hot phases, and are star forming. Collisionless star particles are spawned from gas particles undergoing SF, based on the stochastic scheme by Katz, Weinberg & Hernquist (1996). We allow a gas particle to spawn up to four generations of stars.

Stellar evolution and chemical enrichment feedback are incorporated following the chemical evolution model of Tornatore et al. (2007). Production of 11 species (H, He, C, Ca, O, N, Ne, Mg, S, Si and Fe) are accounted for using detailed yields from Type Ia SN (SN-Ia), Type II SN (SN-II), along with low- and intermediate-mass stars (LIMS) in the thermally pulsating asymptotic giant branch phase. Both SN-Ia and SN-II contribute to thermal feedback. There are mass-dependent time delays with which different stellar populations release metals, adopting the lifetime function by Padovani & Matteucci (1993). Different stellar yields are used: for SN-Ia taken from Thielemann et al. (2003), SN-II from Woosley & Weaver (1995) and LIMS from van den Hoek & Groenewegen (1997). The

---

[1] By *subgrid* we mean *subresolution*, referring to physical processes occurring at length-scales smaller than the resolved scales in our simulations.

mass range for SN-II is considered to be $M/\mathrm{M}_\odot > 8$, while that for SN-Ia originating from binary systems is $0.8 < M/\mathrm{M}_\odot < 8$ with a binary fraction of 10 per cent.

We include a fixed stellar initial mass function (IMF) according to the formalism given by Chabrier (2003), which is a power law at $M/\mathrm{M}_\odot > 1$ and has a log-normal form at masses below. However, we use power-law IMFs with different slopes over the whole mass range of 0.1 to $100\,\mathrm{M}_\odot$, which mimics the log-normal form of Chabrier (2003) at lower masses, as tests indicate. The functional form: $\phi(M) = KM^{-y}$, is composed of three slopes and normalizations: $y = 0.2$ and $K = 0.497$ for stellar masses $0.1 \leq M/\mathrm{M}_\odot < 0.3$, $y = 0.8$ and $K = 0.241$ for $0.3 \leq M/\mathrm{M}_\odot < 1$, and $y = 1.3$ and $K = 0.241$ for $1 \leq M/\mathrm{M}_\odot < 100$. Stars within a mass interval $[8\text{–}40]\,\mathrm{M}_\odot$ become SNe first before turning into BHs at the end of their lives, while stars of mass $>40\,\mathrm{M}_\odot$ are allowed to directly end in BHs.

The chemical evolution model incorporates mass-loss through stellar winds and SNe explosions, which are self-consistently computed for a given IMF and lifetime function. A fraction of a star particle's mass is restored as diffuse gas during its evolution, and distributed to the surrounding gas particles. There is no kinetic feedback from SNe-driven galactic outflows in our simulations. This is because we want to decouple AGN-driven from SNe-driven outflowing gas, and aim to explore uncontaminated outflows driven solely by thermal or kinetic AGN feedback.

2.1 BH accretion and energy feedback

Our subgrid models for BH accretion and feedback are based on the original prescriptions by Springel et al. (2005), which we extend to include kinetic feedback. The mass inflow rate of surrounding gas on to a central SMBH of mass M_{BH} is parametrized by the rate given by Hoyle & Lyttleton (1939), Bondi & Hoyle (1944) and Bondi (1952):

$$\dot{M}_{\mathrm{Bondi}} = \alpha \frac{4\pi G^2 M_{\mathrm{BH}}^2 \rho_\infty}{\left(c_{\mathrm{s},\infty}^2 + v^2\right)^{3/2}}. \tag{1}$$

In the original Bondi–Hoyle–Lyttleton parametrization, ρ_∞ is the gas density far from the BH (or, at infinity), $c_{\mathrm{s},\infty}$ is the sound speed in the gas far from BH, v is the velocity of the BH relative to the far-off gas, and the parameter α is analytically dependent on gas adiabatic index (γ) with $\alpha = 1/4$ for $\gamma = 5/3$. It was originally used to formulate critical astrophysical accretion, where gas is subsonic far away, passes through a sonic point and accretes on to the central object with a supersonic velocity.

The issue of computational resolution appears: current standard galaxy formation simulations resolve kpc to 100's of pc length-scales, hence the Bondi radius and sonic point ($\sim$10's of pc) are unresolved. The gas properties (ρ_∞, $c_{\mathrm{s},\infty}$) used in equation (1) are estimated by smoothing on the resolution scale (smoothing length $>$ a few $100\,\mathrm{pc}$) at the BH location. This results in artificially low densities compared to spatially resolving the Bondi radius scale. Furthermore, smaller scale simulations (Barai, Proga & Nagamine 2012; Gaspari, Ruszkowski & Oh 2013) show that the cooling gas is multiphase, with a variable accretion rate. This cold phase of the ISM is not resolved in galaxy simulations. As a numerical correction, the Bondi–Hoyle–Lyttleton accretion rate inferred from simulations is enhanced by setting the multiplicative factor to $\alpha \sim 100$ (e.g. Springel et al. 2005; Sijacki et al. 2007; Di Matteo et al. 2008; Khalatyan et al. 2008; Johansson, Naab & Burkert 2009a; Sijacki, Springel & Haehnelt 2009; Dubois et al.

2010). Booth & Schaye (2009) used an α factor dependent on the gas density.

The idealized assumptions of the original Bondi theory: spherically symmetric, non-rotating, adiabatic, steady and unperturbed gas flow with constant boundary conditions, has led to recent criticisms of the adopted Bondi accretion model in galaxy simulations. Using analytical arguments and simulating spherical gas distribution within the length-scales (0.001–1) kpc, Hobbs et al. (2012) showed that in free-falling gas due to efficient cooling and gravity of the surrounding halo, the Bondi–Hoyle formalism can be erroneous by orders of magnitude in either direction. In sub-pc resolution simulations where the gas is cooling, Gaspari et al. (2013) and Barai et al. (2012) saw the formation of a multiphase medium, composed of thermal-instability-driven cold clouds and filaments within the hot gas, which makes the accretion cold and chaotic. Gaspari et al. (2013) inferred that the accretion rate is boosted up to two orders of magnitude compared with the Bondi prediction. Such ongoing studies are attempting to improve the BH accretion prescription in intermediate-scale simulations resolving the sonic radius (also Barai, Proga & Nagamine 2011a). Alternate methods have also been prescribed recently to estimate the BH accretion rate on galaxy scales: use viscous transport of angular momentum (Debuhr et al. 2010) and accretion disc particle method (Power, Nayakshin & King 2011; Wurster & Thacker 2013a). Incorporating such modified accretion schemes in full cosmological simulations make up avenues for future work.

Nevertheless despite the limitations, the Bondi model for BH accretion is widely used in galaxy-scale numerical studies, as we do in this work. The accretion rate estimated from the simulations must allow the BHs to grow from seed masses to that observable in the Universe today, within a few Gyr or the Hubble time. It can be analytically shown that a BH, embedded in star-forming gas (having $\rho > \rho_{\mathrm{SF}}$) governed by the Springel & Hernquist (2003) effective equation of state (Section 2), accreting via equation (1) has a mass growth time $t_{\mathrm{g}} \propto 1/\alpha$. The time t_{g} is less than the Hubble time when $\alpha \geq 100$. With a smaller α value, t_{g} exceeds the Hubble time and then it is never possible to grow the BH to the observed masses. Following these arguments to mimic the appropriate growth of BHs in our simulations, we adopt the Bondi–Hoyle–Lyttleton formulation with a constant multiplicative factor $\alpha = 100$.

Furthermore, accretion is limited to the Eddington rate, making the resultant BH mass accretion rate,

$$\dot{M}_{\mathrm{BH}} = \min\left(\dot{M}_{\mathrm{Bondi}}, \dot{M}_{\mathrm{Edd}}\right). \tag{2}$$

Here, $\dot{M}_{\mathrm{Edd}}$ is the Eddington mass accretion rate, expressed in terms of the Eddington luminosity

$$L_{\mathrm{Edd}} = \frac{4\pi G M_{\mathrm{BH}} m_p c}{\sigma_T} = \epsilon_r \dot{M}_{\mathrm{Edd}} c^2. \tag{3}$$

A fraction of the accreted rest-mass energy is considered to be radiated away by the BH, assuming radiatively efficient accretion. The radiation luminosity is

$$L_r = \epsilon_r \dot{M}_{\mathrm{BH}} c^2, \tag{4}$$

with ϵ_r being the radiative efficiency fraction. We adopt the mean value for radiatively efficient accretion on to a Schwarzschild BH (Shakura & Sunyaev 1973): $\epsilon_r = 0.1$, which is kept fixed. This is supported by recent sub-pc resolution simulations of Maio et al. (2013), who found that possible values of radiative efficiencies should be between $0.09 - 0.15$.

A fraction ϵ_f of the radiated energy is eventually fed back to the neighbouring gas as feedback energy from the BH:

$$\dot{E}_{feed} = \epsilon_f L_r = \epsilon_f \epsilon_r \dot{M}_{BH} c^2. \tag{5}$$

Using $\epsilon_f = 0.05$, Di Matteo et al. (2005) found consistent correlation of BH mass and galaxy stellar velocity dispersion (the $M_{BH}-\sigma_\star$ relation), between galaxy merger simulations and observations. We consider the feedback efficiency ϵ_f as a free parameter in our models.

We examine two ways in which the BH feedback energy is coupled to the surrounding gas.

(i) *Thermal*. We adopt the default scheme from Springel et al. (2005). The energy $\dot{E}_{feed}$ is distributed thermally to heat up the gas isotropically around the BH. The temperature of the neighbouring gas particles (those contributing to equation 11 in Section 2.3) is incremented by an amount scaled by their SPH kernel weights. For a gas particle dense enough to be multiphase star forming, the excess specific thermal energy decays to attain the specific energy of the effective equation of state, on a relaxation time-scale τ_h (from equation 12 of Springel & Hernquist 2003):

$$\tau_h = \frac{t_\star \rho_h}{\beta (A + 1) \rho_c}. \tag{6}$$

Here $t_\star$ is the SF time-scale in the effective multiphase model, ρ_h and ρ_c are the densities of hot ambient gas and cold clouds, respectively, β is the mass fraction of stars which are short lived and instantly die as SNe, A is the efficiency of evaporation of cold clouds to be returned to the hot phase due to SNe feedback. If the local cooling time (computed assuming all the particle mass is in the hot phase) is shorter than τ_h, normal radiative cooling is used to dissipate the BH thermal feedback energy.

(ii) *Kinetic*. The gas velocity is increased, as described next.

2.2 Kinetic AGN feedback

In the following, we consider that BH feedback drives a gas outflow of velocity v_w and mass outflow rate $\dot{M}_w$. The energy-conservation equations can be written using the kinetic energy or momentum of the outflowing gas, each of which gives one AGN wind formalism. We consider one fixed value for v_w (a free parameter), which is a simplified assumption of our models (intended to be applied to cosmological simulations in the future), although more physically the AGN wind velocity should be self-regulated (e.g. Gaspari et al. 2011a,b).

2.2.1 Energy-driven wind

The kinetic energy carried away by the wind is equated to the feedback energy from BH:

$$\frac{1}{2}\dot{M}_w v_w^2 = \dot{E}_{feed} = \epsilon_f \epsilon_r \dot{M}_{BH} c^2. \tag{7}$$

This gives the outflow rate as

$$\dot{M}_w = 2\epsilon_f \epsilon_r \dot{M}_{BH} \frac{c^2}{v_w^2}. \tag{8}$$

2.2.2 Momentum-driven wind

Energy output is related to the momentum of radiation via $E = pc$. The rate of momentum outflow in the AGN wind is $\dot{p}_w = \dot{M}_w v_w$. Equating $\dot{p}_w$ to the radiation momentum from AGN we get

$$\dot{p}_w = \dot{M}_w v_w = \frac{\dot{E}_{feed}}{c} = \epsilon_f \epsilon_r \dot{M}_{BH} c. \tag{9}$$

This expresses the mass outflow rate in terms of the BH accretion rate

$$\dot{M}_w = \epsilon_f \epsilon_r \dot{M}_{BH} \frac{c}{v_w}. \tag{10}$$

The main difference between energy-driven wind (EDW) and momentum-driven wind (MDW) is the occurrence of factors $(c/v_w)^2$ and (c/v_w) in the mass outflow rate equations (8) and (10). Hence, to have the same $\dot{M}_w$ in both cases, a larger efficiency factor is needed in MDW: $\epsilon_{f,MDW} = 2\epsilon_{f,EDW}(c/v_w)$.

There are two free parameters in our subgrid model of kinetic feedback: ϵ_f and v_w. Typical AGN wind velocity values seen in observations are between $v_w = $ a few 1000–10 000 km s^{-1}. Debuhr, Quataert & Ma (2012) considered wind velocities of 3000, 7000 and 10 000 km s^{-1} in their simulations of kinetic AGN feedback. The radiative efficiency ϵ_r (equations 3, 4) is held at a fixed value. We vary the free parameters (ϵ_f, v_w) within reasonable ranges to obtain a closest match of the simulation versus observational $[M_{BH}-\sigma_\star]$ relation (Section 3.1), and discuss the best-fitting parameters.

2.3 Implementation in the GADGET-3 code

A BH is represented as a collisionless particle in the GADGET-3 code, having a *dynamical* mass $m_{BH, dyn}$, given by simulation resolution (Section 2.4, Table 1). Owing to the numerics of low- and medium-resolution simulations (where one might need to track BHs in galaxies containing some hundreds of particles), there is another variable describing the BH mass in a smooth fashion, which we call the *subgrid mass*, M_{BH}. The value $m_{BH, dyn}$ is used for the non-AGN physics in the code (e.g. gravitational interactions). M_{BH} is used to compute the AGN physics (e.g. Bondi rate, equation 1), which is hence the true BH mass.

At $t = 0$ in our simulations, the collisionless particle is seeded with a BH having an initial subgrid mass $M_{BH} = M_{BH, seed} = 10^5$ M$_\odot$. At each time step Δt, it grows according to the BH accretion rate (equation 2), its subgrid mass increases by an amount $\dot{M}_{BH}\Delta t$, with $m_{BH, dyn}$ remaining the same. The initial growth from $M_{BH, seed}$ to $m_{BH, dyn}$ occurs in that way, without altering the surrounding gas distribution. After a BH has grown such that $M_{BH} \geq m_{BH, dyn}$, it

Table 1. Galaxy initial conditions. Column 2: virial velocity. Column 3: total mass (dark matter + gas + stars). Column 4: gas mass (disc). Column 5: stellar disc mass. Column 6: stellar bulge mass. Column 7: DM particle mass. Column 8: gas particle mass. Column 9: disc star particle mass. Column 10: BH particle dynamical mass. Column 11: disc (gas + stars) scalelength.

Series name	v_{200} (km s^{-1})	M_{tot} (M$_\odot$)	M_{gas} (M$_\odot$)	$M_{\star,disc}$ (M$_\odot$)	$M_{\star, bulge}$ (M$_\odot$)	m_{DM} (M$_\odot$)	m_{gas} (M$_\odot$)	$m_{\star, disc}$ (M$_\odot$)	$m_{BH, dyn}$ (M$_\odot$)	d (kpc h^{-1})
Low mass	75	1.40×10^{11}	1.12×10^9	4.47×10^9	1.40×10^9	4.42×10^5	2.23×10^4	1.79×10^5	6.98×10^5	1.49
Fiducial	150	1.12×10^{12}	8.93×10^9	3.57×10^{10}	1.12×10^{10}	3.53×10^6	1.79×10^5	1.43×10^6	5.58×10^6	2.99
High mass	300	8.93×10^{12}	7.15×10^{10}	2.86×10^{11}	8.93×10^{10}	2.83×10^7	1.43×10^6	1.14×10^7	4.47×10^7	5.98

might accrete (so-called *swallow*) neighbouring gas particles, using a stochastic methodology. When a gas particle is swallowed, it is removed from the simulation and $m_{BH, dyn}$ increases by the swallowed particle mass m_{gas}. This conserves dynamical mass within the computational volume. The probability of swallowing gas is set to ensure that M_{BH} and $m_{BH, dyn}$ tracks each other closely. Such a procedure grows the BH in a continuous fashion with time, increasing the mass M_{BH} smoothly. It also allows to track BHs less massive than $m_{BH, dyn}$. Having just a single BH mass would create significant fluctuations in $m_{BH, dyn}$ at the epochs when discrete gas particles are accreted, and would render impossible to have a correct BH mass in less massive galaxies.

We do not incorporate any scheme for BH advection (which is done in some studies by e.g. reposition BH at minimum gravitational potential), since our tests obtain a BH dynamics expected for isolated systems. In an isolated galaxy the separation between the BH and the minimum gravitational potential is always less than the softening lengths, while during a merger the BHs deviate from the potential minima by a few times softening some of which is due to merger dynamics.

Kernel-weighted quantities are computed smoothing over gas particles in the local environment around the BH, using a kernel having the same shape as that used in SPH calculations. However, four times more neighbours are used for the BH particle, than in the SPH (which has 32 ± 4 neighbours). The kernel size, or the BH smoothing length s_{BH}, is determined (in analogy to finding gas particle smoothing length) by implicit solution of the equation

$$\frac{4}{3}\pi s_{BH}^3 \rho_{BH} = M_{ngb}. \tag{11}$$

Here, ρ_{BH} is the kernel estimate of the gas density at the position of the BH and M_{ngb} is the mass of $\sim 4 \times 32$ neighbouring gas particles.

We implement a probabilistic criterion (similar to other subgrid prescriptions in GADGET-3) to distribute the kinetic feedback energy from the BH to the neighbouring gas, i.e. particles whose masses contributed to the total neighbour mass M_{ngb} in equation (11). Gas particles are stochastically selected from the neighbours and kicked into AGN wind, by imparting a one-time v_w boost. A probability for being kicked is calculated in a time step Δt for each neighbouring ith gas particle:

$$p_i = \frac{w_i \dot{M}_w \Delta t}{\rho_{BH}}. \tag{12}$$

Here, $w_i = W(|r_{BH} - r_i|, s_{BH})$ is the SPH kernel weight of the gas particle relative to the BH, and $\dot{M}_w$ is the mass outflow rate expressed by equation (8) or (10) for EDW or MDW, respectively. Note that p_i is similar to the probability for swallowing gas particles during BH accretion (Springel et al. 2005). A random number x_i, uniformly distributed in the interval [0, 1], is drawn and compared with p_i. For $x_i < p_i$, the gas particle is given a wind velocity kick. If v_{old} is particle velocity and ϕ its gravitational potential, then after receiving AGN wind kick, its velocity is updated to

$$v_{new} = v_{old} + v_w \hat{x}. \tag{13}$$

The direction given by the unit vector $\hat{x}$ is set along $(v_{old} \times \nabla\phi)$ or $-(v_{old} \times \nabla\phi)$, randomly selected between the two. This makes the wind particles to be preferentially ejected along the rotation axis of the galaxy or perpendicular to the galaxy disc. Some other studies (e.g. Tescari et al. 2011; Barai et al. 2013) implement hydrodynamic decoupling of the wind particles. Unlike those we do not allow any decoupling, i.e. in this work the AGN wind particles are always coupled and undergo hydrodynamic interactions.

The merger criterion of two BHs is when they come inside the s_{BH} of each other, and their relative velocity is smaller than the local sound speed.

2.3.1 Detect hole in gas distribution and prevent its growth

We implement a novel numerical algorithm in the GADGET-3 code to detect and prevent the expansion of hole in the gas distribution around the BH. In the original version, there was a problem of hole creation, classically demonstrated by a BH accreting gas with no feedback at the centre of a rotationally supported disc galaxy. The BH would deplete the central gas, inside its smoothing length, by swallowing particles. In order to have a constant number of neighbours, s_{BH} increases after some time encompassing gas further out. The new gas is depleted in turn, turning the BH more massive, and creating an enlarging hole at the galaxy centre. The process continues ad infinitum, with s_{BH} extending furthermore to accrete the gas of the whole galaxy, unless an upper limit is imposed on s_{BH}. Here, gas is artificially accreted because of the numerical scheme, and not physically because it has flown inward. Observed galaxies do not show any hole in the gas distribution around their central BHs, therefore the creation of such artificial holes affects the simulated evolution of the galaxy and AGN feedback in unwanted ways.

This issue has been present in all the studies using the BH numerical methodology of Springel et al. (2005), demonstrated by the BH growing to $M_{BH} > 10^9\,\mathrm{M}_\odot$ (their fig. 10) in a no-feedback run. A visual example of the hole can be seen in fig. 13 of Wurster & Thacker (2013b).

One solution is to set a maximum s_{BH} manually, which however is not elegant because the value would vary with resolution, galaxy mass and additionally the environment in a cosmological simulation. We have rather worked out a computational solution, to prevent the limitless increase of s_{BH} independent of simulation conditions.

Our numerical methodology assumes that the BH lies at the gas density peak, or minimum SPH smoothing length (s_{sml}) location. The existence of a *hole* around the BH is detected using the s_{sml} distribution of neighbours. With no hole, the minimum s_{sml} occurs at the BH position. When there is a hole, a preferential boundary is created at s_{BH}, with a fewer than expected number of gas particles inside. This causes a small increase in the s_{sml} of neighbours nearest to the BH, and the minimum s_{sml} occurs at a finite distance from the BH location. Also s_{BH} is then more than two times larger than the minimum s_{sml} of neighbours.

In our code implementation, we detect just when a hole is created around a BH and control it. Gas particles lying within a multiplication factor d_h times s_{BH} are searched to find the nearest particle's smoothing length s_{near}, and the minimum smoothing length s_{min}. If either of the following ratio of smoothing lengths exceeds a value r_h:

$$\frac{s_{BH}}{s_{min}} > r_h, \qquad \text{or,} \qquad \frac{s_{near}}{s_{min}} > r_h, \tag{14}$$

then a hole exists. When this *existence-of-hole* condition is met for a BH, its s_{BH} is held fixed, and not allowed to enlarge further. Testing with a single BH in an isolated galaxy we find the working values of factors as: $d_h = 4$ and $r_h = 1.7$. The hole is limited to a size $\sim (0.7$–$0.8)\,h^{-1}$ kpc successfully. All our isolated and merger simulations are done using these values in the hole-detection algorithm.

2.4 Initial galaxy models

The initial isolated galaxy models are constructed following the approach described in Springel & White (1999) and Springel et al.

(2005). The total galaxy mass $M_{\text{tot}} = v_{200}^3/(10\,G\,H_0)$ is expressed in terms of the circular virial velocity v_{200}. A Hubble parameter of $H_0 = 70.3\,\text{km s}^{-1}\,\text{Mpc}^{-1}$, or $h = 0.703$ (e.g. Komatsu et al. 2011), is adopted. Each galaxy is composed of a DM halo, a rotationally supported gaseous and stellar disc comprising of a fraction $f_{\text{d}} = 0.04$ of the total mass, and a central stellar bulge of mass fraction $f_{\text{b}} = 0.01$. The mass distribution of the DM halo is modelled with the Hernquist (1990) profile, and has a spin parameter of $\lambda = 0.04$. The disc has a mass fraction $f_{\text{gas}} = 0.2$ as gas, and the rest as stars; both components are modelled with an exponential surface density profile of radial scalelength d and radially constant vertical scaleheight $z_0 = 0.2\,d$. The spherical stellar bulge is modelled with a Hernquist (1990) profile having a scalelength $b = 0.2\,d$.

We simulated galaxies of three masses. Our fiducial galaxy is generated using $v_{200} = 150\,\text{km s}^{-1}$, which corresponds to $M_{\text{tot}} = 1.12 \times 10^{12}\,\text{M}_{\odot}$, a similar mass as the Milky Way. Furthermore, we simulate galaxies having a lower mass with $v_{200} = 75\,\text{km s}^{-1}$ and a higher mass with $v_{200} = 300\,\text{km s}^{-1}$. The number of particles of various types in the initial condition of each galaxy are: 3×10^5 DM, 5×10^4 gas, 25×10^3 disc stars and 25×10^3 bulge stars. Table 1 lists the relevant mass components and particle masses of all the galaxies. New star particles form during the simulation (via SF in the gas), which are less massive than the initial stellar particles in the disc and bulge. All the particles (DM, gas and stars) follow collisionless gravitational dynamics, while in addition the gas particles undergo hydrodynamical interactions.

A collisionless tracer particle of mass fraction $f_{\text{BH}} = 5 \times 10^{-6}$ is generated at the centre of a galaxy to *carry* the SMBH. This corresponds to a dynamical BH particle mass ($5.58 \times 10^6\,\text{M}_{\odot}$ in our fiducial galaxy) which is $\sim$1.6 times higher than the DM particle mass. The BH particle is thus expected to trace the minimum of the gravitational potential closely, minimizing artificial dynamical motion. In the AGN simulations, a BH of initial subgrid mass $10^5\,\text{M}_{\odot}$ is seeded in this tracer particle.

The Plummer-equivalent softening length for gravitational forces is set to $L_{\text{soft}} = 0.5/h\,\text{kpc}$ for the gas and star particles, and $1/h\,\text{kpc}$ for the DM and BH particles. The minimum SPH smoothing length is set to a fraction 0.001 of L_{soft}.

As the initial conditions for the merger simulations, two equal-mass isolated galaxies are generated using a fixed v_{200}. The orbital planes of the two discs are kept the same, and they are set on a parabolic collision course in the disc plane. A minimum separation at which the galaxies would pass at pericentre (if they were point masses) is taken as $2.5/h$, $5/h$ and $10/h\,\text{kpc}$, respectively, for the lower mass, fiducial and higher mass cases.

2.5 Simulations

Table 2 lists the series of simulations we perform. The different runs incorporate the same non-AGN subgrid physics described in Section 2 and investigate different AGN feedback models. They are chosen from four broad categories, as given below, exploring the model parameter space.

(i) *SF*. One run with SF, stellar evolution and chemical enrichment only (no BH).

(ii) *th1–th3*. Three runs of thermal feedback from BH (Section 2.1), using $\epsilon_{\text{f}} = 0.002$, 0.01 and 0.05.

(iii) *kinE1–kinE6*. Six runs of kinetic feedback from BH with EDW prescription (Section 2.2.1), using combinations of $\epsilon_{\text{f}} = 0.01$, 0.05, 0.25, and $v_{\text{w}} = 5000$, 10 000 km s^{-1}.

(iv) *kinM1–kinM4*. Four runs of kinetic feedback from BH with MDW prescription (Section 2.2.2), using combinations of $\epsilon_{\text{f}} = 0.25$, 1.0, and $v_{\text{w}} = 1000$, 2500, 5000 km s^{-1}.

The fiducial galaxy ($v_{200} = 150\,\text{km s}^{-1}$) is simulated using all the above parameter cases for both isolated galaxy evolution (indicated by letter 'I' in Table 2, columns 5, 6, 7) and galaxy merger (indicated by letter 'M' in Table 2). The parameter set of each category which generates a closest fit to observations is also run with the lower mass ($v_{200} = 75\,\text{km s}^{-1}$) and higher mass ($v_{200} = 300\,\text{km s}^{-1}$) galaxy models. The isolated galaxies are evolved up to a time 2 Gyr and the galaxy mergers up to 3 Gyr.

3 RESULTS AND ANALYSIS

We compare the BH mass (M_{BH}) versus galaxy stellar velocity dispersion ($\sigma_{\star}$) results obtained in our simulations with the observed correlation, using a manual chi-by-eye approach. This comparison is considered as the figure of merit in order to obtain the best-fitting parameters for each AGN feedback model. The fiducial galaxy ($v_{200} = 150\,\text{km s}^{-1}$) is simulated using several parameter variations in a series of runs (Section 2.5), each for isolated and merger evolution. The parameter set of each category which generate a closest fit to the observational $[M_{\text{BH}}-\sigma_{\star}]$ relation at the fiducial galaxy mass are selected. These chosen cases are also run with the lower mass ($v_{200} = 75\,\text{km s}^{-1}$) and higher mass ($v_{200} = 300\,\text{km s}^{-1}$) galaxy models.

All the runs performed are presented in Section 3.1. For the galaxy morphologies in Section 3.2, we choose models generating a comparable BH mass, i.e. the BHs in these cases exist in the same region of the $[M_{\text{BH}}-\sigma_{\star}]$ diagram. Consequently, we compare between thermal and kinetic feedback with different ϵ_{f}, because the respective best-fitting ϵ_{f} are unequal. Results in remaining sections only show the closest fit models, plus a few cases with varying ϵ_{f} and v_{w}. Note that our approach explores parameters which fit the $[M_{\text{BH}}-\sigma_{\star}]$ relation. This however renders difficult to perform an absolute comparison of thermal versus kinetic feedback, since the respective output powers are different, as described in Section 3.3.

We analyse the carbon content of the gas in the galaxies, since it is one of the most abundant heavy element in the Universe, and the spectral lines produced by ionized carbon are relatively easy to observe. The carbon metallicity, Z_{C}, is computed as the ratio of carbon mass to the total particle mass for each gas particle. Abundance ratios are expressed in terms of the solar metallicity, which is $Z_{\text{C},\odot} = 0.002\,177$ (mass fraction of carbon in Sun) derived from the compilation by Asplund, Grevesse & Sauval (2005).

3.1 $[M_{\text{BH}}-\sigma_{\star}]$ correlation

The galaxy stellar velocity dispersion $\sigma_{\star}$ is computed by considering all the stars: those newly formed during the simulation evolution by SF from gas, the disc and bulge stellar components present from the initial condition (Section 2.4, Table 1). The position of the BH is taken as the galaxy centre, and the distances (or radii) of star particles are estimated from it. In the case of merging galaxies the calculations are done at a time when the BHs have merged to produce a single BH, defining a unique galaxy centre. The cumulative sum of all star's mass versus radius is found, as well as the radius $R_{1/2}$ containing 1/2 of the total stellar mass. This stellar half-mass radius is considered as the effective radius in estimating $\sigma_{\star}$. 100 random line-of-sight (LOS) directions are chosen around the centre (or, BH position). All the stars lying within $R_{1/2}$ from the centre are

Table 2. Simulation parameters. Column 1: name of simulation run. Column 2: feedback efficiency, ϵ_f = fraction of the radiated energy from BH which is coupled to the surrounding gas. Column 3: v_w = outflow velocity in kinetic feedback prescription. Column 4: specifications of AGN feedback model. Columns 5, 6, 7: letters 'I' (isolated galaxy evolution) and/or 'M' (galaxy merger) are written below lower mass ($v_{200} = 75\,\mathrm{km\,s^{-1}}$), fiducial ($v_{200} = 150\,\mathrm{km\,s^{-1}}$) and higher mass ($v_{200} = 300\,\mathrm{km\,s^{-1}}$) galaxy models, wherever the parameter set in the row has been run with the column initial configuration.

Run name	ϵ_f	v_w (km s^{-1})	AGN feedback	Lower mass	Fiducial	Higher mass
SF			No BH		I, M	
th1	0.002		BH thermal		I, M	
th2	0.01		BH thermal	I	I, M	I
th3	0.05		BH thermal	M	I, M	M
kinE1	0.01	5000	BH kinetic: EDW		I, M	
kinE2	0.05	5000	BH kinetic: EDW	I	I, M	I
kinE3	0.25	5000	BH kinetic: EDW	M	I, M	M
kinE4	0.01	10 000	BH kinetic: EDW		I, M	
kinE5	0.05	10 000	BH kinetic: EDW		I, M	
kinE6	0.25	10 000	BH kinetic: EDW	I, M	I, M	I, M
kinM1	0.25	5000	BH kinetic: MDW		I, M	
kinM2	1.0	5000	BH kinetic: MDW		I, M	
kinM3	1.0	2500	BH kinetic: MDW	I	I, M	I
kinM4	1.0	1000	BH kinetic: MDW		M	

picked and the LOS velocity component of each, v_{LOS}, is found. The stellar velocity dispersion along each LOS direction is computed by summing over all relevant stars

$$\sigma_\star = \left(\langle v_{\mathrm{LOS}}^2 \rangle - \langle v_{\mathrm{LOS}} \rangle^2 \right)^{1/2}. \tag{15}$$

The same is done for the 100 LOS directions. The median and percentile of the 100 random direction $\sigma_\star$ values are found and shown as our results.

Fig. 1 presents the M_{BH} versus $\sigma_\star$ diagram obtained in our simulations. The left-hand panel shows the isolated galaxy cases at an evolution time 2 Gyr. The right-hand panel shows the galaxy merger runs at a time 2.5 Gyr, an epoch by when the two BHs merge in all the cases. The median $\sigma_\star$ is depicted by the plotting symbol and 70th percentiles around the median are indicated by the lower and upper error bars. Observational data are overplotted in Fig. 1 as the straight lines. The solid and dashed lines display the best-fitting relations and error bars obtained by Tremaine et al. (2002) are shown in black and Gultekin et al. (2009) in orange.

The best-fitting parameters that we obtain for the isolated galaxy evolution are: for BH thermal feedback $\epsilon_f = 0.01$; for BH kinetic EDW feedback $v_w = 5000\,\mathrm{km\,s^{-1}}$ with $\epsilon_f = 0.05$ and $v_w = 10\,000\,\mathrm{km\,s^{-1}}$ with $\epsilon_f = 0.25$; and for BH kinetic MDW feedback $v_w = 2500\,\mathrm{km\,s^{-1}}$ with $\epsilon_f = 1$. Estimating by-eye the nearness of the simulation result to the observational $[M_{\mathrm{BH}}-\sigma_\star]$ relation at a given galaxy mass, we find mass dependence of the relative fit given by a set of parameters, more prominently for the isolated galaxy than the merger case. The final BH masses of the four best-fitting cases tend to be relatively smaller than the observations for the higher mass galaxy and larger than the observations for the lower mass galaxy.

We obtain the following best-fitting parameters for the galaxy merger: for BH thermal feedback $\epsilon_f = 0.05$; and for BH kinetic EDW feedback $v_w = 5000$ or $10\,000\,\mathrm{km\,s^{-1}}$ with $\epsilon_f = 0.25$. For BH kinetic MDW feedback, none of the parameters we explored fit the observations; the BH mass is always too large. In the case of other feedback models, M_{BH} reduces when ϵ_f is increased (thermal,

kinetic EDW), also when v_w is decreased (kinetic EDW). However, there is a reversal of trends with kinetic MDW; at $v_w = 5000\,\mathrm{km\,s^{-1}}$ M_{BH} decreases as the efficiency rises from $\epsilon_f = 0.25$ to 1, but M_{BH} increases rather as v_w is reduced further to $2500\,\mathrm{km\,s^{-1}}$. Even when ϵ_f is set to 1, the smallest BH mass produced is $M_{\mathrm{BH}} \sim 2.5 \times 10^8\,\mathrm{M_\odot}$ with $v_w = 5000\,\mathrm{km\,s^{-1}}$ in a fiducial galaxy run. With $v_w = 1000\,\mathrm{km\,s^{-1}}$ the BH grows drastically to $M_{\mathrm{BH}} \sim 2 \times 10^9\,\mathrm{M_\odot}$. This happens because in the merging system such a velocity is not high enough to remove the gas away, but the kicked gas falls back near the BH(s) and is accreted. Thus, we find that it is not possible to find ϵ_f and v_w values to fit the observational $[M_{\mathrm{BH}}-\sigma_\star]$ relation with MDW prescription of BH kinetic feedback in the case of a galaxy merger.

3.2 Galaxy morphology and outflow

The galaxy morphology and outflow structure of three representative isolated cases are plotted in Fig. 2 at an evolution time 1.73 Gyr. It is a fiducial galaxy with different feedback models: *SF* (left two columns) – SF only, *th1* (middle two columns) – BH thermal feedback with $\epsilon_f = 0.002$ and *kinE1* (right two columns) – BH kinetic feedback EDW with $\epsilon_f = 0.01$, $v_w = 5000\,\mathrm{km\,s^{-1}}$. In the latter two runs the BHs grow to a comparable mass $M_{\mathrm{BH}} \sim 1.5 \times 10^7\,\mathrm{M_\odot}$ (from Fig. 1).

The gas disc of the galaxy retains its identity in all the runs, visible as a well-defined rotating disc in the central $r = (10\text{--}20)\,h^{-1}\,\mathrm{kpc}$ regions. There is no outflow in the *SF* case. Thermal feedback (run *th1*) produces a weak outflow with some gas going out to $(30\text{--}40)\,h^{-1}\,\mathrm{kpc}$, but later in time most of the outflowing gas fall back to the disc. Kinetic feedback (edge-on plane of *kinE1*) produces a well-developed bipolar gas outflow propagating perpendicular to the galaxy disc, escaping to $r > 100\,\mathrm{kpc}$ from the central BH position, seen in the topmost-right panel, as the red arrows upward and downward directed.

The gas density, temperature and carbon metallicity are plotted in the second, third and fourth rows of Fig. 2, respectively. All the runs
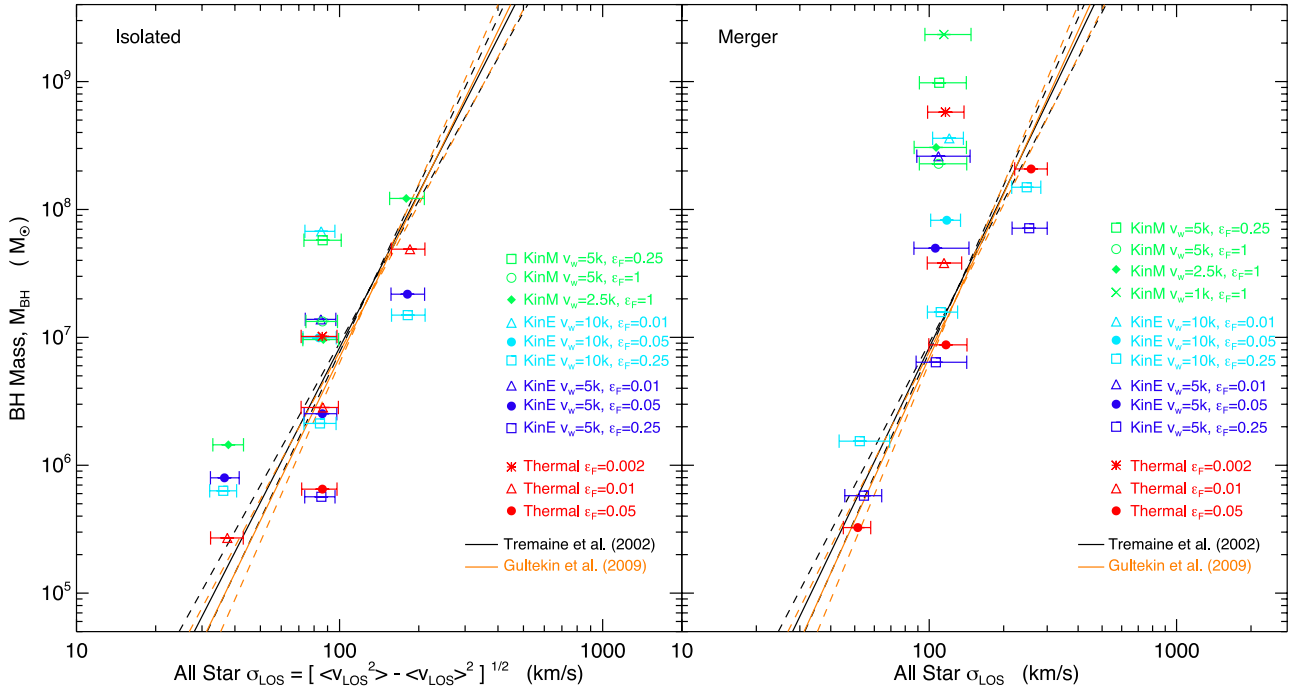
Figure 1. BH mass versus galaxy stellar velocity dispersion along LOS. The single isolated galaxy models, shown at an evolution time of 2 Gyr, are in the left-hand panel. The merger simulations, shown at an evolution time of 2.5 Gyr, are in the right-hand panel. The different colours and plotting symbols distinguish the AGN models as labelled in each panel. Each of the four broad categories of feedback is denoted by a different colour: [*th1–th3*] thermal – red, [*kinE1–kinE3*] kinetic EDW with $v_w = 5000\,\mathrm{km\,s^{-1}}$ – blue, [*kinE4–kinE6*] kinetic EDW with $v_w = 10\,000\,\mathrm{km\,s^{-1}}$ – cyan, [*kinM1–kinM4*] kinetic MDW – green. The parameter choices are represented by the plotting symbols: $\epsilon_f = 0.002$ – asterisk, $\epsilon_f = 0.01$ – triangle, $\epsilon_f = 0.05$ – filled circle, $\epsilon_f = 0.25$ – open square, $\epsilon_f = 1$ – open circle, $\epsilon_f = 1$ and $v_w = 2500\,\mathrm{km\,s^{-1}}$ – filled diamond, $\epsilon_f = 1$ and $v_w = 1000\,\mathrm{km\,s^{-1}}$ – cross. The solid and dashed lines display the best-fitting relations and error bars obtained from observations by Tremaine et al. (2002) – black and Gultekin et al. (2009) – orange.

have a central overdense region, the outer half of which corresponds to a cold, annular ring composed of gas cooling in the disc, on the way to SF. There is a large central concentration of metals, originating from SF, in all the runs. The metallicity distribution is more centrally concentrated in *SF* and *th1* cases. Kinetic feedback carries some metals out from the SF regions and enrich the CGM and IGM to $>100\,\mathrm{kpc}$. A remarkable spiral pattern is visible in the face-on Z_C distribution in the fourth row, fifth column panel.

The bottom row of Fig. 2 depicts the projected stellar mass, where all stars (disc, bulge, newly formed in simulation from gas particles by active SF) have been counted. The edge-on plane shows the co-existence of a disc-like and a bulge-like stellar components. The star distribution is indistinguishable between the three runs.

Fig. 3 presents the projected distributions of gas and stars in the fiducial galaxy merger with three representative models: *SF* (left two columns) – SF only, *th3* (middle two columns) – BH thermal feedback with $\epsilon_f = 0.05$ and *kinE3* (right two columns) – BH kinetic feedback EDW with $v_w = 5000\,\mathrm{km\,s^{-1}}$ and $\epsilon_f = 0.25$. In the latter two runs the BHs grow to a comparable mass $M_{BH} \sim 7 \times 10^6\,\mathrm{M_\odot}$ (from Fig. 1). The intermittent gas outbursts produced by BH kinetic feedback, which were clearly distinguishable in the isolated galaxy, are difficult to disentangle in a merger, because other dynamical processes related to the merger process cause substantial gas to outflow.

The top two rows ($t = 1.59\,\mathrm{Gyr}$) of Fig. 3 depict an epoch when the galaxies are approaching each other, on the way to their second pericentre passage and subsequent coalescence. Earlier at $t \sim 0.4\,\mathrm{Gyr}$ the merging galaxy pair goes through a first pericentre passage during which there is a grazing collision of the outer discs. The resulting shocks and tidal interactions cause some gas to leave

the disc plane and outflow, in all the models including the *SF* case. BH feedback induces enhanced gas outflow: more in run *th3* than *SF*, and highest in run *kinE3*. Each merging galaxy in all the runs exhibit spiral patterns composed of overdense gas. The spiral patterns are somewhat disturbed with kinetic BH feedback. The stellar distribution is almost indistinguishable between the feedback models here at 1.59 Gyr.

The bottom two rows ($t = 2.31\,\mathrm{Gyr}$) of Fig. 3 show the resulting merged galaxy at an epoch during coalescence. It consists of a central compact spheroid and two tidal tails of overdense gas (visible as red in the third row, tails more prominent in *SF* and *th3* runs). There is a diffuse gaseous halo larger in size, which is more spherically shaped in the *SF* case, and quite disturbed giving an irregular appearance with kinetic feedback. The stellar distribution display a few differences between the models at 2.31 Gyr: central 30 h^{-1} kpc radius of the face-on panels exhibit more spherically shaped structure in the *SF* case, then *th3*, and more elliptically shaped in *kinE3*.

3.3 Black hole accretion rate, feedback power and star formation rate

The BH mass accretion rate is an important quantity in the models, which governs BH growth as well as provides feedback energy in a self-regulated manner. It is measurable in observations, which can be compared to simulation results. The time evolution of Black Hole Accretion Rate (BHAR) in our fiducial isolated galaxy is presented in Fig. 4, top-left panel. At $t = 0$, we find an accretion surge of $0.002\,\mathrm{M_\odot\,yr^{-1}}$ because of our simulation initial condition. Embedding a $10^5\,\mathrm{M_\odot}$ BH in the gas-rich environment of a disc galaxy centre suddenly, results in a high accretion rate. It reduces
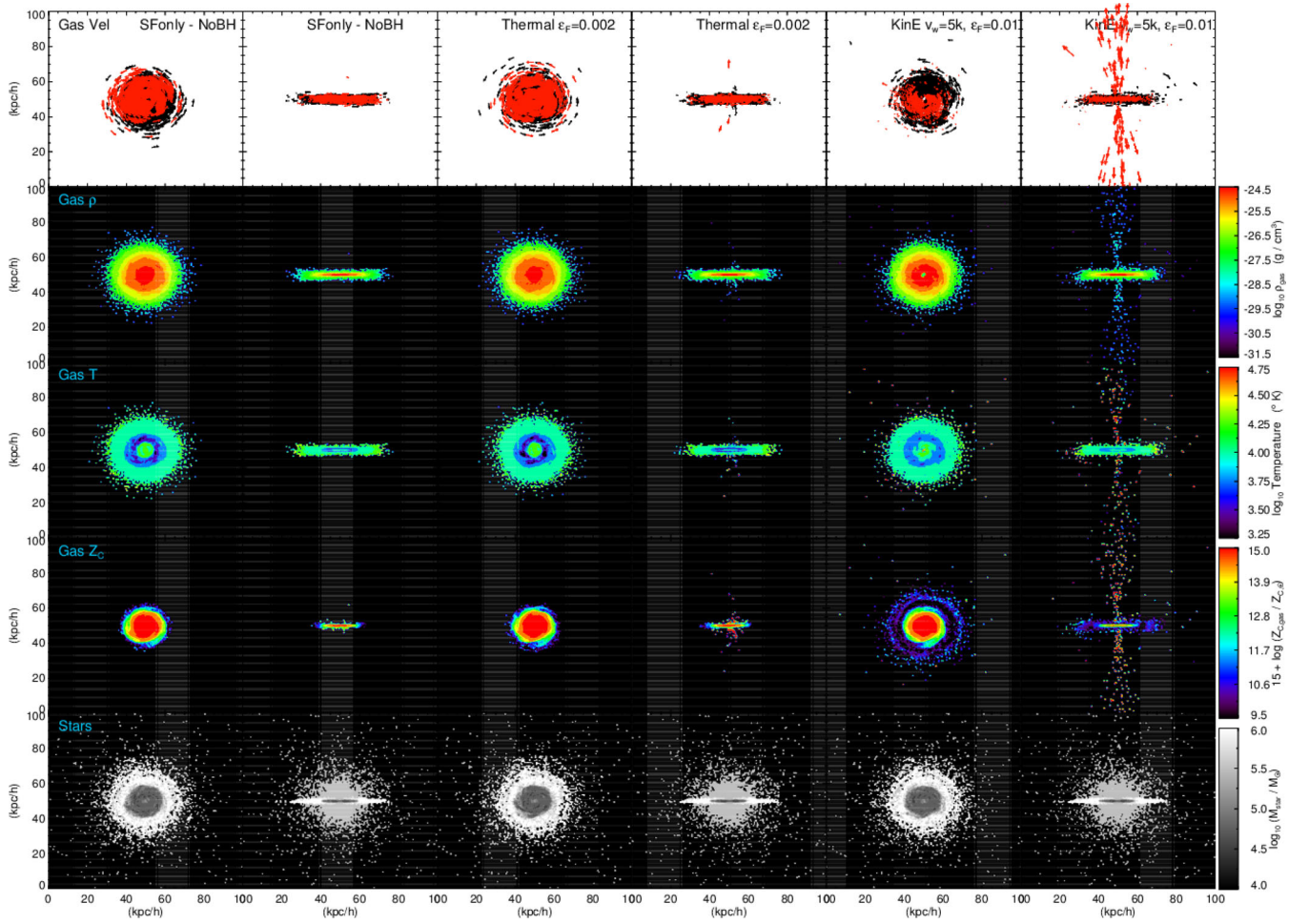
Figure 2. Projection of gas kinematics (top four rows) and stars (bottom row) in isolated fiducial galaxy simulation with different feedback models: *SF* (left two columns) – SF only, *th1* (middle 2 columns) – BH thermal feedback with $\epsilon_f = 0.002$ and *kinE1* (right two columns) – BH kinetic feedback EDW with $\epsilon_f = 0.01$, $v_w = 5000$ km s^{-1}. The panels show the face-on (left) and edge-on (right) planes of a $(100\,h^{-1}\,\mathrm{kpc})^3$ volume centred around the BH (or collisionless tracer particle in the *SF* run) at time $t = 1.73$ Gyr. First row depicts the velocity vectors of 20 per cent of all the gas particles within the projected volume, with the outflowing ($v_r > 0$) particles denoted as red and the inflowing ($v_r < 0$) as black. Second row shows gas density, third row is gas temperature and fourth row is gas carbon metallicity, all projected values, colour coded from red as the highest and black as the lowest. Bottom row presents the projected stellar mass, counting all stars (disc + bulge + newly formed in simulation).

by 100 times soon after, because of reduced central gas, which has depleted by the initial burst of accretion and SF. From 0.02 Gyr, the BHAR rises linearly up to a time $(0.5-0.7)$ Gyr to reach a few times $0.001-0.01\,\mathrm{M_\odot\,yr^{-1}}$, the duration coinciding with the exponential mass growth of the BH (Section 3.4, Fig. 5 top-left panel). There are heavy fluctuations in the BHAR, whereby it increases or decreases by a factor of up to 100 in 0.02 Gyr. The BHAR in terms of the Eddington mass accretion rate (equation 3) also displays significant variability, especially at $t > 0.5$ Gyr. $\dot{M}_{\mathrm{BH}}/\dot{M}_{\mathrm{Edd}}$ varies between $10^{-3}-1$ for the thermal feedback models, while between $10^{-5}-1$ for kinetic.

The feedback energy rate ($\dot{E}_{\mathrm{feed}}$, equation 5) is plotted in Fig. 4, middle-left panel. As expected the feedback power has same trends as BHAR; however, the absolute value of $\dot{E}_{\mathrm{feed}}$ is different depending on ϵ_f. At $t < 0.5$ Gyr, when the BH mass is small, higher ϵ_f produces a larger power. For the same feedback model, the impact of varying ϵ_f reduces at $t > 0.5$ Gyr, as the BHs grow, and the BHAR becomes a dominating factor in $\dot{E}_{\mathrm{feed}}$.

The total star formation rate (SFR) in the fiducial isolated galaxy versus time is displayed in the bottom-left panel of Fig. 4. Similar

to BHAR, at $t = 0$ there is an initial burst of SFR of $6\,\mathrm{M_\odot\,yr^{-1}}$. It reduces afterward via depletion of central gas, and then increases again. The SFR decreases linearly after 0.5 Gyr, as more gas in the galaxy is converted to stars, to reach $1.5\,\mathrm{M_\odot\,yr^{-1}}$ at 2 Gyr. There are periodic fluctuations in the SFR, when it would decrease by a factor of $(1.1-2)$, occurring because of SNe feedback in the stellar evolution model. All the AGN models show these general trends similarly. Thermal feedback produces almost the same SFR as the *SF* run. Kinetic feedback, more prominently the EDW models, produce up to 1.5 times lower SFR than the *SF* and thermal cases at $t > 0.9$ Gyr.

The top-right panel of Fig. 4 depicts the BH mass accretion rate time evolution in the fiducial galaxy merger, with the rates summed over each of the two merging BHs initially when they are separate. Note that the parameter values of the plotted line styles are different between isolated and merger cases. Most of the features of the BHAR in the merger are same as that of the isolated. The amplitude of fluctuations (change by a factor of up to 1000 in 0.02 Gyr) is larger in a merger than isolated case, because of extra dynamical processes (tidal forces, shocks) acting on the two merging galaxies.
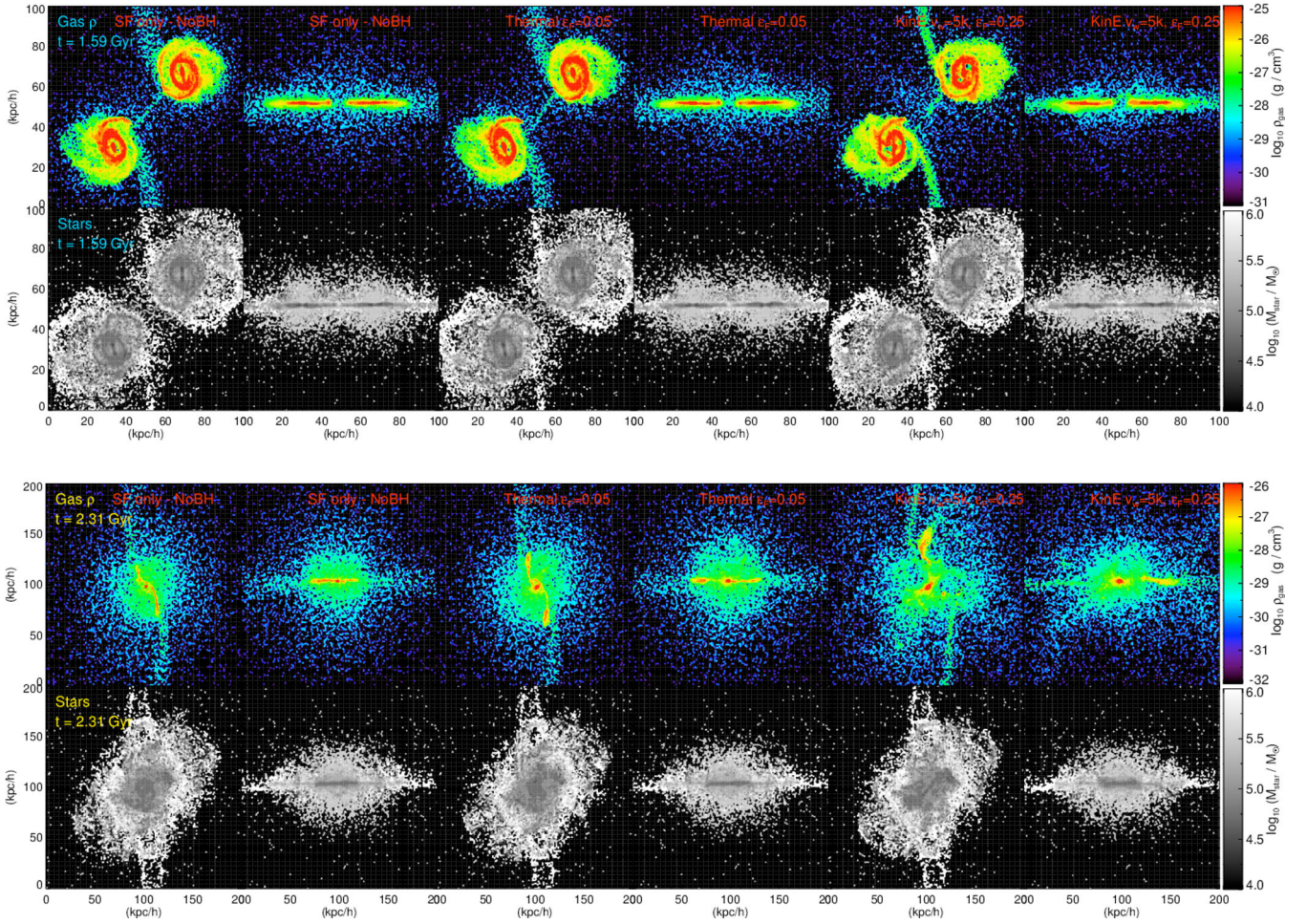
Figure 3. Projection of gas distribution and stars in fiducial galaxy merger simulation with different feedback models: *SF* (left two columns) – SF only, *th3* (middle two columns) – BH thermal feedback with $\epsilon_f = 0.05$ and *kinE3* (right two columns) – BH kinetic feedback EDW with $v_w = 5000$ km s^{-1} and $\epsilon_f = 0.25$. The panels show the face-on (left) and edge-on (right) planes of a $(100\,h^{-1}\,\mathrm{kpc})^3$ volume at time 1.59 Gyr in the top two rows and a $(200\,h^{-1}\,\mathrm{kpc})^3$ volume at $t = 2.31$ Gyr in the bottom two rows. Projected gas density is plotted in the first and third rows, and projected total stellar mass in the second and fourth rows.

The vertical dashed and solid black lines in the right-hand panels of Fig. 4 mark the epochs of first ($t \sim 0.36$ Gyr) and second ($t \sim 1.86$ Gyr) pericentre passages of the two galaxies, which occur at a concurrent time for the different feedback models. The galaxies merge at the second pericentre epoch, while the BHs undergo a third and some subsequent pericentres before merging.

The feedback power in the merger is in Fig. 4, middle-right panel. Its dependence on BHAR and ϵ_f is similar to that in an isolated galaxy.

The bottom-right panel of Fig. 4 shows the total SFR in the fiducial merger versus time, with the rates summed over each of the two galaxies. The initial features of the SFR in the merger case are the same as that of the isolated. The stellar evolution induced fluctuations have larger amplitudes at $t > 1$ Gyr in a merger than an isolated galaxy. The SFR decreases linearly from 0.9 Gyr to (1.6−1.7) Gyr reaching a local minimum depending on the AGN model. It rises subsequently because of additional gas inflow to dense central regions of the merging galaxies, and passes through a local peak at $t = 1.86$ Gyr during the second pericentre passage. It reaches another peak at (2.1−2.2) Gyr, and decreases henceforth by gas depletion. At $t > 2$ Gyr, thermal feedback (red curves) produces lower SFR than the *SF* run (black curve) by a factor between (1.5−10). Kinetic feedback causes a greater suppression of SFR,

starting from 0.9 Gyr; the reduction factors with respect to the *SF* case are: 5−30 times in EDW models with $v_w = 5000$ km s^{-1} (blue) and in MDW models (green), 10−100 times for EDW models with $v_w = 10\,000$ km s^{-1} (cyan).

3.4 Galaxy mass components

The masses of BH and gas components in the isolated fiducial galaxy models versus evolution time is plotted in Fig. 5. The left-hand panel presents the BH mass, where all the feedback models have the BH growing in a qualitatively similar manner. Starting from a seed mass of 10^5 M$_\odot$, each BH first undergoes a slow growth. It then has an exponential growth over the time range (0.5−1) Gyr, when its mass increases by a factor of 10 to a few 100. After 1 Gyr it comes to an almost steady state, having a very slow subsequent growth. The final BH mass reached at 2 Gyr depends on the AGN model, and is inversely proportional to ϵ_f and directly proportional to v_w. A higher ϵ_f imparts a stronger feedback affecting more central gas, and yields a less massive BH than a lower ϵ_f. On increasing v_w, $\dot{M}_w$ decreases (inverse proportionality in equation (8) for EDW and (10) for MDW), there is reduced kinetic feedback and less gas is ejected out, making more gas available for accreting on to BH which grows
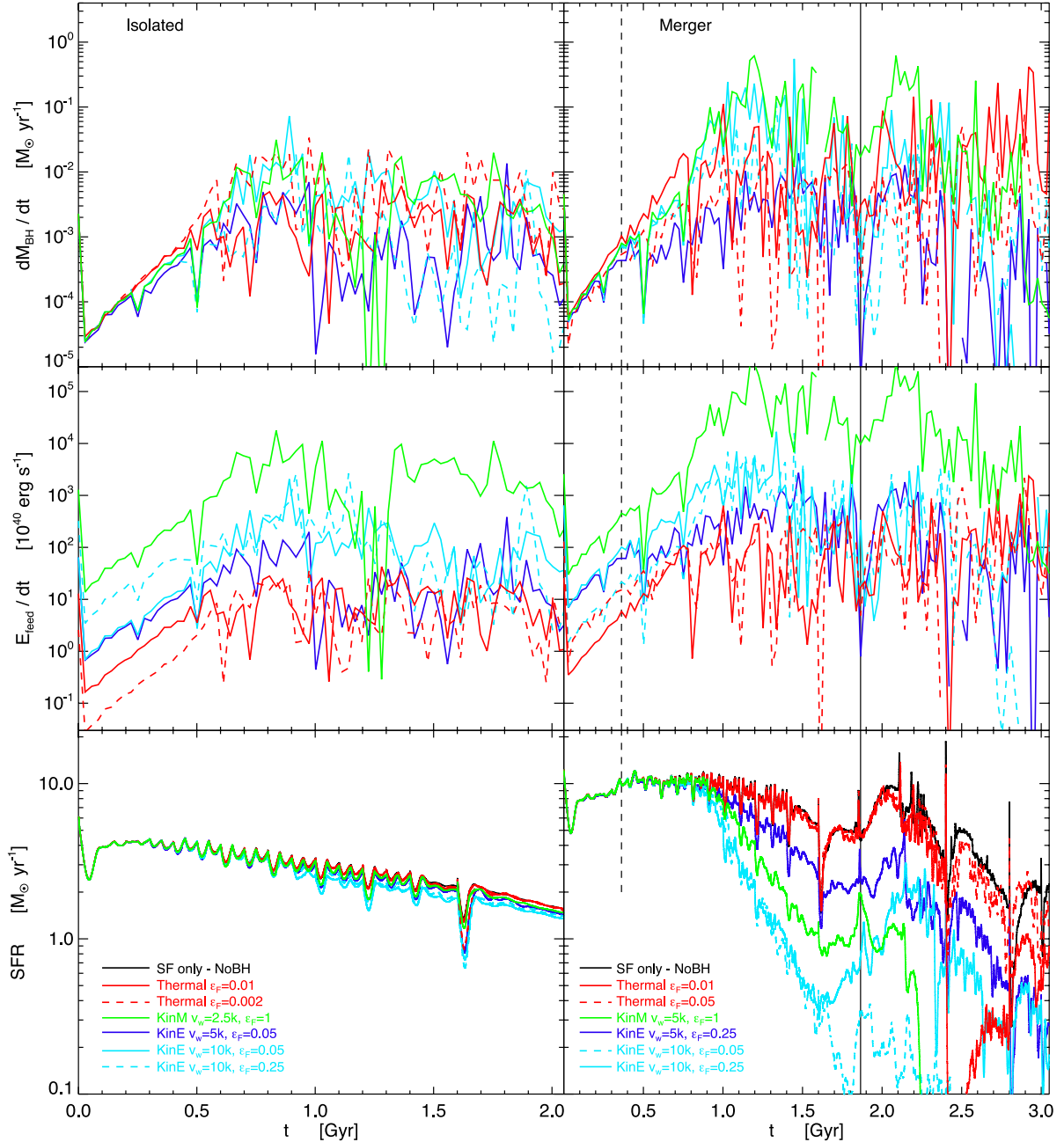
Figure 4. Evolution with time of BH mass accretion rate (top row), energy feedback rate (middle row) and total SFR (bottom row), in the fiducial case of isolated galaxy (left column), and merger (right column) simulations. The different colours and plotting line styles discriminate AGN feedback models labelled in the bottom panels. The runs for a single isolated galaxy are: *SF* (black solid) – SF only, *th1* (red dashed) – thermal with $\epsilon_f = 0.002$, *th2* (red solid) – thermal with $\epsilon_f = 0.01$, *kinE2* (blue solid) – kinetic EDW with $v_w = 5000\,\mathrm{km\,s^{-1}}$ and $\epsilon_f = 0.05$, *kinE5* (cyan solid) – kinetic EDW with $v_w = 10\,000\,\mathrm{km\,s^{-1}}$ and $\epsilon_f = 0.05$, *kinE6* (cyan dashed) – kinetic EDW with $v_w = 10\,000\,\mathrm{km\,s^{-1}}$ and $\epsilon_f = 0.25$, *kinM3* (green solid) – kinetic MDW with $v_w = 2500\,\mathrm{km\,s^{-1}}$ and $\epsilon_f = 1$. The contributions from each of the two merging galaxies are summed over, and the resulting total rates are plotted in the right-hand column. Note that the parameter values of the plotted line styles are different between isolated and merger cases. The galaxy merger runs are: *SF* (black solid) – SF only, *th2* (red solid) – thermal with $\epsilon_f = 0.01$, *th3* (red dashed) – thermal with $\epsilon_f = 0.05$, *kinE3* (blue solid) – kinetic EDW with $v_w = 5000\,\mathrm{km\,s^{-1}}$ and $\epsilon_f = 0.25$, *kinE5* (cyan dashed) – kinetic EDW with $v_w = 10\,000\,\mathrm{km\,s^{-1}}$ and $\epsilon_f = 0.05$, *kinE6* (cyan solid) – kinetic EDW with $v_w = 10\,000\,\mathrm{km\,s^{-1}}$ and $\epsilon_f = 0.25$, *kinM2* (green solid) – kinetic MDW with $v_w = 5000\,\mathrm{km\,s^{-1}}$ and $\epsilon_f = 1$. The vertical dashed black line in the right-hand panels marks the epoch of first pericentre passage of the two merging galaxies, and the vertical solid black line marks the second pericentre passage.

more massive. As a note, a BH which is only accreting gas with no feedback grows to a mass of $3 \times 10^8\,\mathrm{M_\odot}$ in 2 Gyr.

The right-hand panel of Fig. 5 depicts the gas mass which has outflown, or that lying outside a pre-defined disc region. No gas outflows in the *SF* run. In the case of thermal feedback a tiny

fraction ($< 10^{-3}$) of gas outflows after 1 Gyr. The kinetic feedback models cause some gas to outflow starting from (0.2 to 0.3) Gyr. The outflowing mass rises exponentially during the peak period of BH growth, because the feedback energy governing the mass outflow is derived from the BH accretion rate. A few $\times 10^8\,\mathrm{M_\odot}$ gas has
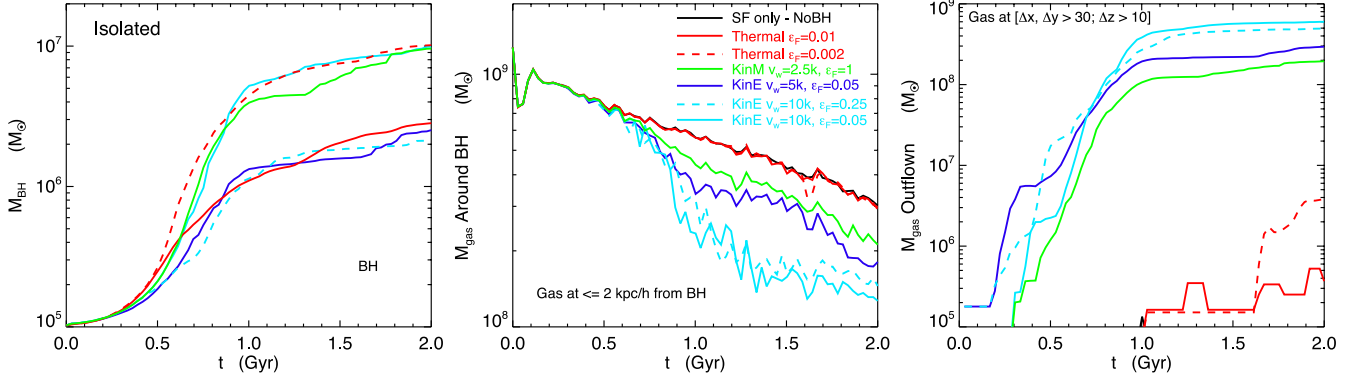
Figure 5. Time evolution of component masses in isolated galaxy simulation, fiducial model: BH mass (left-hand panel), gas mass inside distance $r \leq 2\,h^{-1}$ kpc from BH (middle), gas mass outflown or that outside Δx, $\Delta y > 30\,h^{-1}$ kpc and $\Delta z > 10\,h^{-1}$ kpc (right). The distinguishing colours and plotting line styles indicate different AGN feedback models: *SF* (black solid) – SF only, *th1* (red dashed) – BH thermal feedback with $\epsilon_f = 0.002$, *th2* (*red solid*) – BH thermal feedback with $\epsilon_f = 0.01$, *kinE2* (blue solid) – BH kinetic feedback EDW with $v_w = 5000\,\mathrm{km\,s^{-1}}$ and $\epsilon_f = 0.05$, *kinE5* (cyan solid) – BH kinetic feedback EDW with $v_w = 10\,000\,\mathrm{km\,s^{-1}}$ and $\epsilon_f = 0.05$, *kinE6* (cyan dashed) – BH kinetic feedback EDW with $v_w = 10\,000\,\mathrm{km\,s^{-1}}$ and $\epsilon_f = 0.25$, *kinM3* (green solid) – BH kinetic feedback MDW with $v_w = 2500\,\mathrm{km\,s^{-1}}$ and $\epsilon_f = 1.0$.

outflown by 1 Gyr, which is a fraction $0.03-0.07$ of the initial gas mass.

The middle panel of Fig. 5 denotes the time evolution of central gas. This summed mass inside $r \leq 2\,h^{-1}$ kpc from the BH consists of the innermost gas which is accreted on to the BH, ejected out by kinetic feedback, and is part of the central high-density star-forming region of the galaxy where gas is converted to stars. This mass decreases equally for all the feedback models up to ~ 0.7 Gyr, which is an impact of SF, and the BH mass is still small. Thermal feedback does not alter the central gas reservoir content. In the

kinetic models, the inner gas is depleted such that the central mass becomes $0.25-0.5$ of the *SF* case between $(1-2)$ Gyr. There the BH grows appreciably after 0.5 Gyr, exerts strong kinetic feedback and ejects the central gas out.

Fig. 6 displays the time evolution of various component (BH, gas, stars)'s masses in the fiducial merger simulation. The mass contribution from each of the two merging galaxies is summed over, and the resulting total masses are plotted. Some trends are similar to the isolated galaxy evolution in Fig. 5, while some are different caused by the dynamics of the merger process.
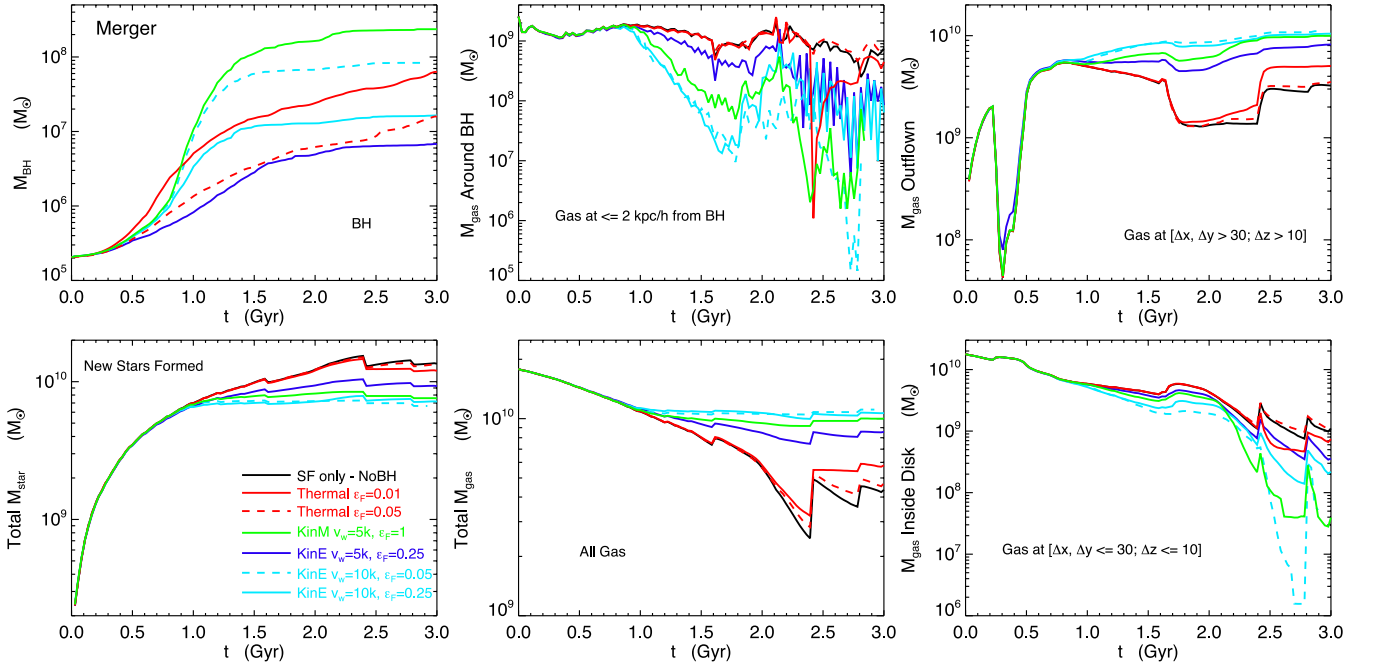

Figure 6. Time evolution of various component (BH, gas, stars)'s masses in galaxy merger simulation, fiducial model: BH mass (top-left panel), gas mass inside $r \leq 2\,h^{-1}$ kpc from BH (top middle), gas mass outflown (top right), mass of new stars formed from gas (bottom left), total gas mass in galaxy (bottom middle), gas mass inside disc (bottom right). The mass component for each of the two merging galaxies are summed over, and the resulting total masses are plotted. The different colours and plotting line styles distinguish between AGN feedback models: *SF* (black solid) – SF only, *th2* (red solid) – BH thermal feedback with $\epsilon_f = 0.01$, *th3* (red dashed) – BH thermal feedback with $\epsilon_f = 0.05$, *kinE3* (blue solid) – BH kinetic feedback EDW with $v_w = 5000\,\mathrm{km\,s^{-1}}$ and $\epsilon_f = 0.25$, *kinE5* (cyan dashed) – BH kinetic feedback EDW with $v_w = 10\,000\,\mathrm{km\,s^{-1}}$ and $\epsilon_f = 0.05$, *kinE6* (cyan solid) – BH kinetic feedback EDW with $v_w = 10\,000\,\mathrm{km\,s^{-1}}$ and $\epsilon_f = 0.25$, *kinM2* (green solid) – BH kinetic feedback MDW with $v_w = 5000\,\mathrm{km\,s^{-1}}$ and $\epsilon_f = 1.0$.

The BH mass in the top-left panel of Fig. 6 shows a similar general trend as isolated galaxy. The steady state reached at $t > 1.5$ Gyr, after the exponential growth, is more prominent with kinetic feedback than thermal. The impact of varying v_w is reduced in a merger than a single isolated galaxy.

The mass of new stars formed (bottom-left panel of Fig. 6) increases overall, and the total gas mass in the galaxies (bottom middle) decreases with simulation time over $(0-3)$ Gyr, for all the AGN models, as gas is converted to stars and is accreted on to central BH. Except there are some epochs (at $\sim$1.2, 1.6, 2.4 and 2.8 Gyr) when the star mass reduces and gas mass increases by the same amount, occurring because of stellar mass-loss (a part of the stellar evolution model of Tornatore et al. 2007). Thermal feedback produces a late visible impact; at $t > 2$ Gyr there is slightly smaller star mass and a higher gas mass than the *SF* case. The influence of kinetic feedback is larger, visible from 1.1 Gyr; the stellar mass is reduced by a factor of $1.7-2.5$ than *SF*, resulting in a correspondingly higher gas mass.

The bottom-right panel of Fig. 6 shows the gas mass inside a disc region, within distances from central BH Δx, $\Delta y \leq 30\,h^{-1}$ kpc along the disc plane and $\Delta z \leq 10\,h^{-1}$ kpc in the perpendicular direction. At $t > 1$ Gyr, the kinetic feedback cases have a smaller disc mass than the *SF* and thermal runs, occurring because of increased outflows.

The top-right panel of Fig. 6 denotes the gas mass which has outflown, i.e. lying outside the disc region. Contrary to the isolated case, in the merger of two galaxies there is significant gas outflow from the beginning, for all the models. The *SF* run has $3 \times 10^9\,\mathrm{M_\odot}$ gas outflow by 3 Gyr, a few times larger than the gas mass within the disc at the same time. This no-feedback outflow occurs mainly because of shock heating and collisions during the merger. In the case of thermal feedback the outflown gas mass is up to two times higher than the *SF* case at $t > 2$ Gyr. The kinetic feedback models expel a significantly higher fraction of gas than the *SF* and thermal runs; $\sim 10^{10}\,\mathrm{M_\odot}$ gas outflows by 3 Gyr, which is comparable or larger than the mass of new stars formed and $(100-1000)$ times higher than the gas mass remaining in the disc. Thus, the resulting galaxy, produced by the merger of two disc galaxies, contains most of its gas in the form of an extended spheroidal halo.

The rearrangement of gas distribution in the two galaxies during the merger is indicated by a few opposite trends in the component evolution. The outflow mass (top-right panel of Fig. 6) decreases sharply at 0.3 Gyr, coinciding with a rise in disc mass (bottom right). This corresponds to the first pericentre passage (marked in the right-hand panels of Fig. 4) of the galaxies approaching each other. During this encounter, tidal forces cause more gas to flow inward. After 0.5 Gyr the galaxies move apart, restoring the original gas configuration in each. They undergo a second pericentre passage starting at $\sim$1.6 Gyr, when the outflow mass reduces and disc mass increases again. The galaxy discs collide during this passage, the disc structures are lost in the violent encounter, some gas recoil forming tidal tails, and the nuclear regions merge between $(2-2.5)$ Gyr, making a galaxy with spheroidal gas distribution.

The top-middle panel of Fig. 6 shows the central gas evolution, inside $r \leq 2\,h^{-1}$ kpc from the BH in each galaxy. It shows heavy fluctuations at $t > 1$ Gyr; falling because of accreting on to BH and/or ejecting out by feedback and merger shock heating, while rising again when there is gas inflow to the inner regions. The thermal feedback and *SF* cases are almost coincident up to 2.4 Gyr, after which a strong burst of feedback reduces the central gas mass and increases the outflow mass in the *th2* run. In the kinetic models, the inner gas is depleted more at 1.5 Gyr, replenished again later, presenting oscillatory behaviour between $(1.5-3)$ Gyr; finally the central mass becomes $(0.1-0.01)$ of the *SF* case at 3 Gyr.

We see, from Figs 4, 5 and 6, that thermal feedback produces negligible impact compared to the *SF* case in the isolated galaxy and at $t < 2.4$ Gyr in the merger. We investigate and infer that this is because the thermal energy injected is radiated away very quickly by the dense star-forming gas particles in the multiphase model (Springel & Hernquist 2003).

3.5 Radial profiles

The radial profiles of gas properties of the isolated galaxy cases at an evolution time of 2 Gyr are presented in Fig. 7. The radius is computed by the distance from the maximum gas density location. The total galaxy mass varies between the three columns: lower mass of $M_{\rm tot} = 1.40 \times 10^{11}\,\mathrm{M_\odot}$ (left), fiducial of $M_{\rm tot} = 1.12 \times 10^{12}\,\mathrm{M_\odot}$ (middle) and higher mass of $M_{\rm tot} = 8.93 \times 10^{12}\,\mathrm{M_\odot}$ (right). Fig. 8 displays the radial gas profiles of the merged galaxy at $t = 2.31$ Gyr, an epoch when there is still significant gas left near the centre, however, the two BHs in a few runs have not merged yet. The total mass of an individual galaxy undergoing merger varies between the three columns. The profiles of the different models vary, more in the merged galaxy than in the isolated evolution. This is because of the distinct operation of each feedback, affecting the gas in diverse ways enhanced by a merger.

3.5.1 Density

The gas density radial profiles are plotted in the top rows. The isolated models in Fig. 7 exhibit similar density profiles, except the lower mass galaxy, where strong kinetic feedback in the *kinE6* run expels large amounts of gas and reduces the density by 10–100 times than the other runs.

In the merger, Fig. 8, the lower mass and fiducial galaxies present qualitatively similar profiles. However, there are two exceptions in the fiducial galaxy: at $r \sim 3\,h^{-1}$ kpc the *kinE6* case produces a local peak, while the *SF* run generates a local drop. In the inner $r < 2\,h^{-1}$ kpc, the *SF* case exhibits a $\sim$1.5 times higher density than that with thermal feedback, which in turn is $(3-5)$ times denser than those with kinetic feedback. The differences reduce and/or reverse in the outer $r > (2-3)\,h^{-1}$ kpc, where in the lower mass galaxy kinetic feedback causes $\sim$10 times more density than thermal. The higher mass galaxy (top-right panel of Fig. 8) has a smaller density than either of the two other galaxies. This implies that most of the gas has been expelled at 2.31 Gyr here by strong feedback effects.

The features are signatures of kinetic feedback being able to expel gas efficiently from central regions, consequently reducing the central gas density and depositing the gas at larger distances.

3.5.2 Temperature

The temperature radial profiles are presented in the middle rows of Figs 7 and 8, using the effective temperature for those gas particles which are star forming. The T profiles in the inner regions $r \leq (1-2)\,h^{-1}$ kpc of all the galaxies follow the negative-sloped density profiles (top rows in respective figures). This represents the dense gas at galaxy centre undergoing SF, and having a T between $\sim(10^3-5 \times 10^5)$ K, which is directly proportional to the density, as a result of following the SF effective equation of state in the multiphase model by Springel & Hernquist (2003).

In the isolated (Fig. 7) kinetic feedback runs (except case *kinE2* in the higher mass galaxy), the gas T increases with radius at $r > (5-10)\,h^{-1}$ kpc, as the high-velocity outflows thermalize their energies
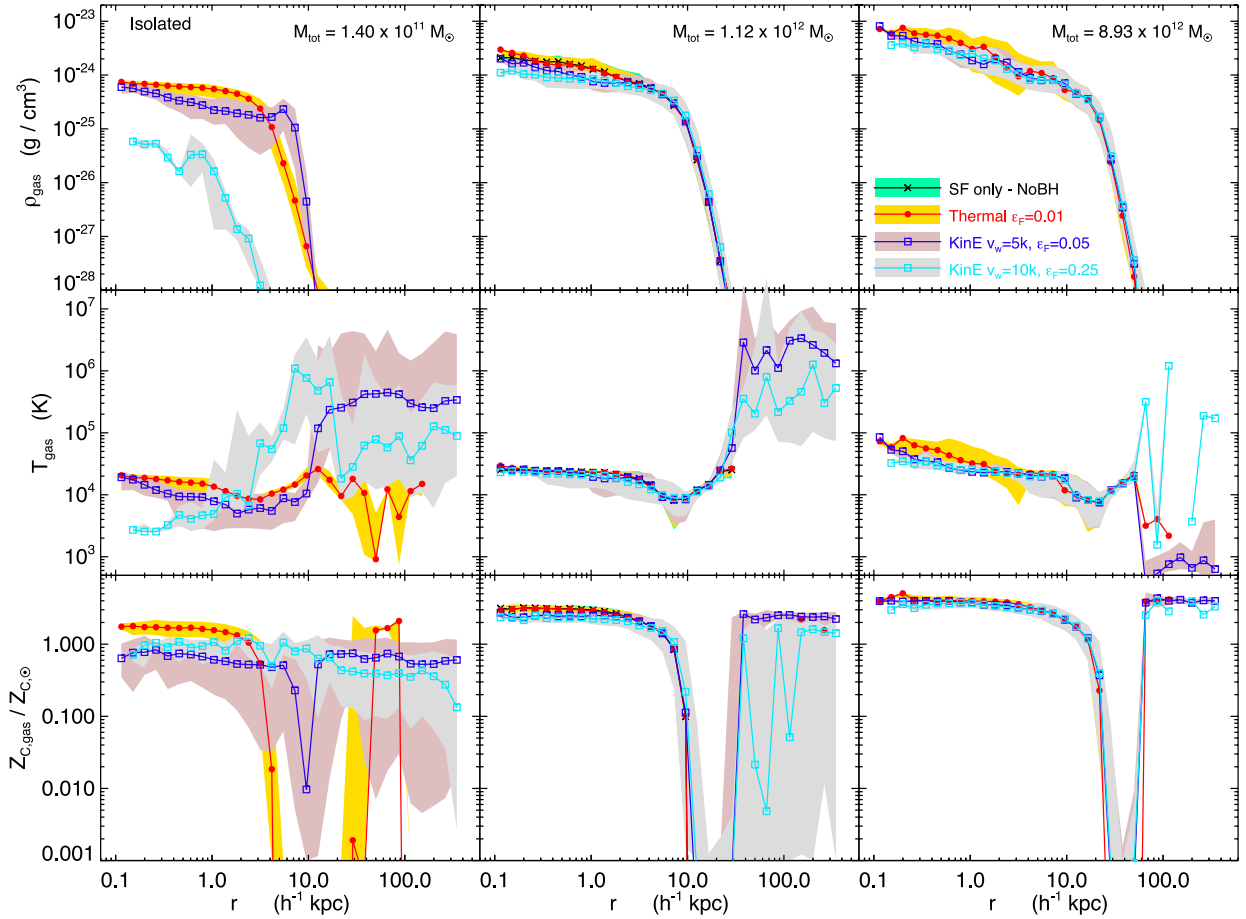
Figure 7. Radial gas profiles of isolated galaxy models at an evolution time of 2 Gyr. The three columns indicate varying total galaxy mass: lower mass with $v_{200} = 75\,\mathrm{km\,s^{-1}}$ and $M_{tot} = 1.40 \times 10^{11}\,\mathrm{M_\odot}$ (left), fiducial with $v_{200} = 150\,\mathrm{km\,s^{-1}}$ and $M_{tot} = 1.12 \times 10^{12}\,\mathrm{M_\odot}$ (middle) and higher mass with $v_{200} = 300\,\mathrm{km\,s^{-1}}$ and $M_{tot} = 8.93 \times 10^{12}\,\mathrm{M_\odot}$ (right). The AGN feedback models providing best fit in the $[M_{BH} - \sigma_\star]$ diagram of an isolated case are plotted: *SF* (black cross, green shade) – SF only, *th2* (red filled circle, yellow shade) – thermal with $\epsilon_f = 0.01$, *kinE2* (blue square, reddish grey shade) – kinetic EDW with $v_w = 5000\,\mathrm{km\,s^{-1}}$ and $\epsilon_f = 0.05$, *kinE6* (cyan square, grey shade) – kinetic EDW with $v_w = 10\,000\,\mathrm{km\,s^{-1}}$ and $\epsilon_f = 0.25$. The plotted curves denote the median quantity in radial bins of each run. The respective shaded areas enclose the 70th percentiles above and below the median in each case, showing the radial scatter. Top row is the gas density in cgs units. Middle row is gas temperature, and the effective equation-of-state T is shown for the multiphase gas particles. Bottom row is carbon metallicity, showing the ratio of carbon mass fraction in gas to that of the Sun.

at large radii. The T profiles reveal that thermal BH feedback does not heat up the inner gas to higher temperatures as a physical model should do.

The fiducial merged galaxy (Fig. 8) *SF* case has a smaller (than the feedback runs) cold central spheroidal core, surrounded by a hot gas halo of size $r \sim 3\,h^{-1}$ kpc; and a prominent cold annular ring at $r \sim (4\text{–}6)\,h^{-1}$ kpc composed of gas infalling from two tidal tails. The gas T increases with radius at $r \geq 2\,h^{-1}$ kpc. These outer regions contain gas shock heated during the merger, and feedback processed material: gas heated by BH thermal coupling and shock heating via kinetically kicked gas. The T profiles show a local peak, which for the *SF* and thermal feedback occurs at a radius (e.g. $r \sim 15\,h^{-1}$ kpc in the fiducial galaxy) 10 times smaller than the kinetic feedback models ($r \sim 200\,h^{-1}$ kpc). This is because the jet-like outflows of kinetic feedback deposit their energies at a larger radii.

3.5.3 Carbon metallicity

Radial profiles of the ratio of carbon mass fraction in the gas to that of the Sun are plotted in the bottom rows of Figs 7 and 8. The medians and percentiles are computed considering all (both enriched and non-enriched) gas particles in radial bins. In the isolated galaxy (Fig. 7) the Z_C profiles are flat overall. It has a sharp decrease at a mass-dependent radii corresponding to the end of the galaxy disc, and increases again at larger radii in the feedback runs comprising of metal-enriched gas ejected out.

In the merged galaxy (Fig. 8), the kinetic feedback models produce an almost flat, no-gradient Z_C profile in the inner $r < 20\,h^{-1}$ kpc; and small gradients at $r > 20\,h^{-1}$ kpc. These features demonstrate that kinetic feedback is substantially effective in transporting metals away from central SF regions, and spreading them in the lower density surrounding CGM. The *SF* and thermal feedback cases exhibit metallicity gradients at all r in the lower mass and fiducial galaxies. Thermal feedback in the higher mass galaxy produces a no-gradient flat Z_C profile like the kinetic models, with comparable metallicity values. This implies that thermal feedback is relatively more efficient to enrich the CGM of higher mass galaxies.

In the inner $r < 0.5\,h^{-1}$ kpc all the feedback models generate a 1.5 times lower Z_C than the *SF* case, because of suppression of central SF. The trend reverses in the outer $r > 0.5\,h^{-1}$ kpc: thermal feedback displays a higher Z_C up to 10 times more than *SF*, and the
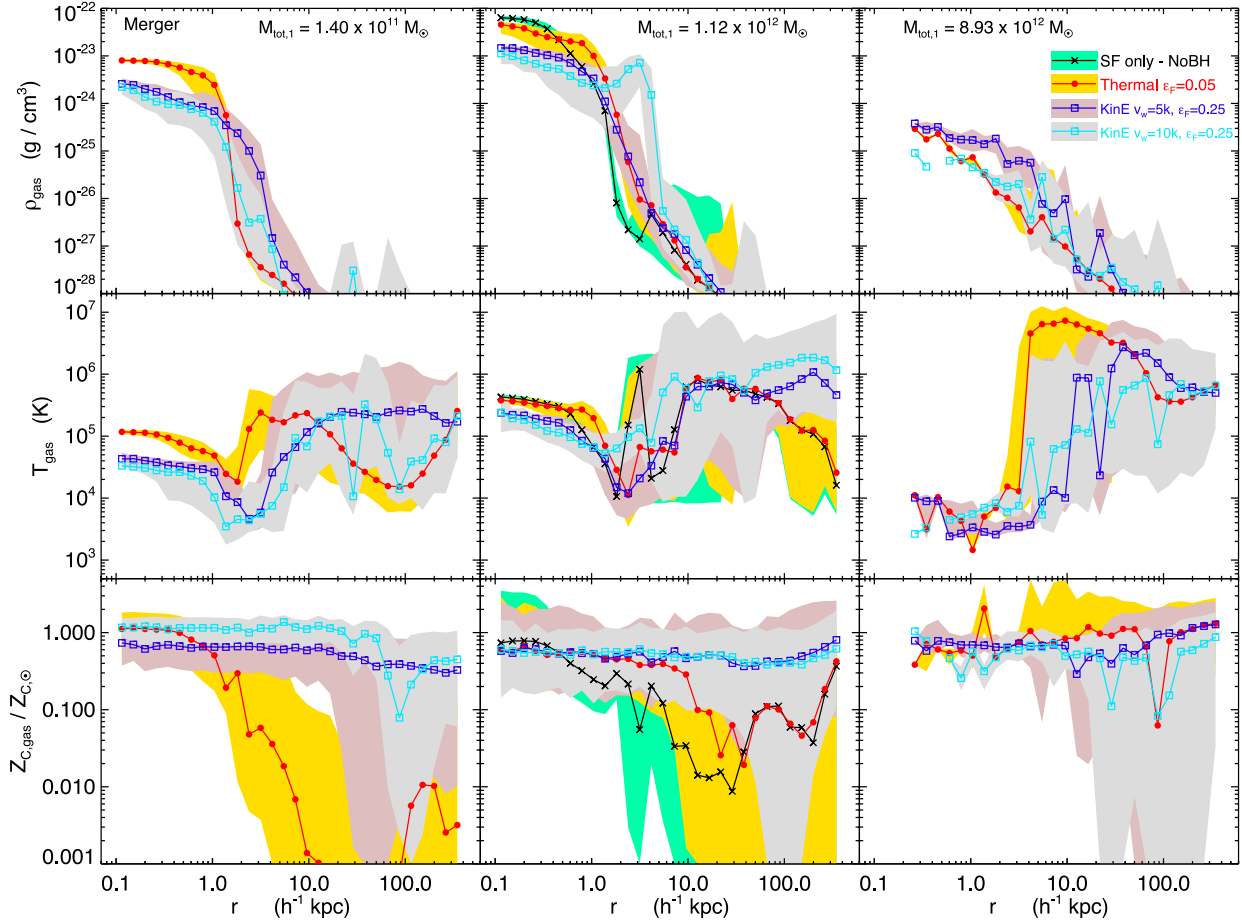
Figure 8. Radial gas profiles of merged galaxy at an evolution time of 2.31 Gyr. The three columns indicate varying total mass of an individual galaxy undergoing merger. The AGN feedback models providing best fit in the [$M_{BH}-\sigma_\star$] diagram of a merger are plotted: *SF* (black cross, green shade) – SF only, *th3* (red filled circle, yellow shade) – thermal with $\epsilon_f = 0.05$, *kinE3* (blue square, reddish grey shade) – kinetic EDW with $v_w = 5000 \, \mathrm{km \, s^{-1}}$ and $\epsilon_f = 0.25$, *kinE6* (cyan square, grey shade) – kinetic EDW with $v_w = 10\,000 \, \mathrm{km \, s^{-1}}$ and $\epsilon_f = 0.25$. The plotted curves denote the median quantity in radial bins of each run, and the shaded areas enclose the 70th percentiles above and below the median. Top row is gas density, middle row is gas temperature (with the effective T shown for the multiphase gas particles) and bottom row is carbon metallicity.

kinetic cases exhibit up to 60 times higher Z_C, originating from the accumulation of metal-enriched gas expelled by feedback.

4 DISCUSSION

We see that BH kinetic feedback operates intermittently, driving bipolar outflows visible for short times. The geometry of the outflowing gas varies with time and feedback model: from jet-like, perfectly collimated fast gas outflows, to wide-angled relatively slower outflows. Sometimes precession of the jets are visible. The variety of outflow geometry can be seen as movies in the given weblink.[2] The jet-like collimated outflows efficiently pierce through the galaxy ISM and escape out perpendicular to the disc. The jets are not perturbed by the environment, since there is no ambient gas outside the galaxy disc in our isolated cases. Effects like mass entrainment, bending and fragmenting of the AGN jets become important in different environments, e.g. for central galaxies in clusters.

The rightmost column of Fig. 2 represents a typical jet-like outburst example. When gas accumulates near the galaxy centre, the

BHAR rises and feedback acts to eject gas out of the disc, consisting of multitemperature, metal-enriched outflow, moving at a high speed v_w. This depletes (partially) the central gas reservoir, and the BHAR reduces, stopping the bipolar outflow. During the off-period, which occurs for a longer time than the outflow was on, gas flows in near the BH again. The process acts periodically with intermittent active outbursts, separated by longer quiescent intervals. Whereas for BH thermal feedback, the outflow occurs relatively more continuously, and after a while some of the outflowing gas slows down, reverses and inflows.

In cosmological simulations, wind particles are often ejected perpendicular to the galaxy disc to generate bipolar outflows, e.g. that done for SNe-driven kinetic feedback (Tescari et al. 2009; Barai et al. 2013). We follow the same for AGN kinetic feedback here (Section 2.3). As a test we perform a new run where the wind particles are ejected isotropically. We find that in isolated galaxies (higher resolution here than in typical cosmological simulations), the effectiveness of kinetic feedback is almost equivalent for bipolar versus isotropic wind ejection. The BHAR, SFR, stellar mass and BH mass remains the same. The isotropic case ejects more central gas outside the disc (≤ 1.3 times the mass than in the bipolar case), because the wind kicked along the galaxy disc interacts with more gas. Note that in our subgrid models the BHAR is the modified

---

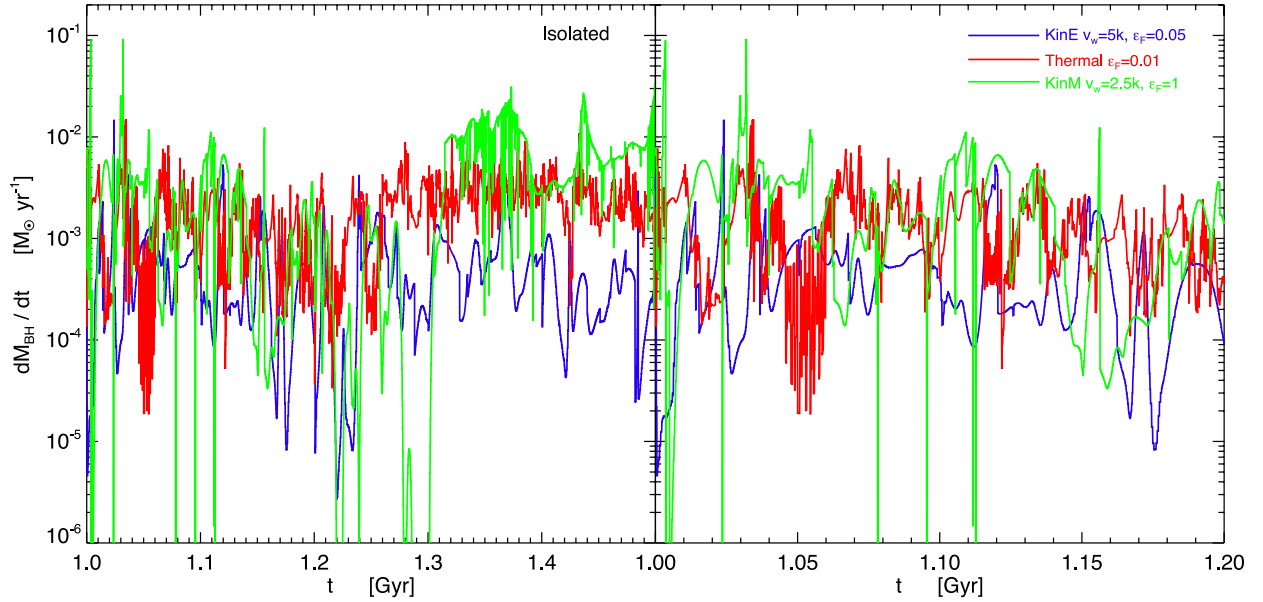[2] http://adlibitum.oats.inaf.it/barai/AllPages/Visualization/Isolated_Galaxy_AGN.html

Figure 9. Evolution with time of BH mass accretion rate in the fiducial isolated galaxy runs, showing zoomed-in time intervals: (1–1.5) Gyr in the left-hand panel and (1–1.2) Gyr in the right. The values at a finer time resolution (every time step of simulation) are plotted, so that all variations are visible as spikes. The colours discriminate AGN feedback models as labelled: *th2* (red) – thermal with $\epsilon_f = 0.01$, *kinE2* (blue) – kinetic EDW with $v_w = 5000\,\mathrm{km\,s^{-1}}$ and $\epsilon_f = 0.05$, *kinM3* (green) – kinetic MDW with $v_w = 2500\,\mathrm{km\,s^{-1}}$ and $\epsilon_f = 1$.

Bondi rate (equation 1), without any check on the radial velocity direction (Section 2.1).

We find the BH mass accretion rate to be highly variable on a range of time-scales. The top-left panel of Fig. 4 presents the BHAR over the whole evolution time (0–2) Gyr, in our fiducial isolated galaxy simulations. Fig. 9 depicts the evolution through zoomed-in time intervals: (1–1.5) Gyr in the left-hand panel and (1–1.2) Gyr in the right. The BHAR values plotted in Fig. 9 are taken from every time step of the simulations, hence are at a finer time resolution than in Fig. 4. Therefore, each and every variation is visible as a separate spike here in Fig. 9. Overall, kinetic feedback causes larger amplitude of the fluctuations (variability factor between 10–10^4) than thermal (up to 100). At $t > 1$ Gyr with kinetic feedback, the accretion spikes of amplitude $\sim$100 have a period of $\sim$0.05 Gyr. Our results are consistent with other studies which find variability of the BHAR in simulations (e.g. Gaspari et al. 2012b; Gabor & Bournaud 2013).

We infer that different model parameters are needed to fit the $[M_{BH}-\sigma_\star]$ observations for a BH evolving in an isolated galaxy versus that formed in a merger of two galaxies. Also varying modes of AGN feedback (thermal versus kinetic, additional details of wind prescription) require different parameter sets. BHs growing in cosmological environments undergo several major and minor mergers as well as quiescent evolution at different epochs. BHs also have alternate phases of feedback, quasar mode versus radio mode (which are usually realized as thermal or kinetic forms of feedback in simulations), at varying points of their lifetimes likely dependent on environment as well. The selection of a unique parameter set for cosmological simulations is hence not straightforward. We find that the best-fitting ϵ_f is larger in a merger than in an isolated galaxy, considering either thermal or kinetic feedback. Furthermore, a larger ϵ_f is needed in kinetic over thermal within each of isolated or merger case.

The obtained trend of larger efficiency for kinetic feedback is consistent with studies using the value $\epsilon_f = 0.15$ in the quasar mode

(Booth & Schaye 2009; Dubois et al. 2013a) and $\epsilon_f = 1$ in the radio mode (Dubois et al. 2013a), which were calibrated to reproduce the Magorrian et al. (1998) relations at $z = 0$. Our best-fitting parameter set [$v_w = 10\,000\,\mathrm{km\,s^{-1}}$, $\epsilon_f = 0.25$] of BH kinetic feedback EDW falls within the $[M_{BH}-\sigma_\star]$ best-fitting category for both isolated galaxy and merger. We plan to explore such parameters in full cosmological simulations in the future.

Our results indicate that faster winds require higher ϵ_f to produce the same BH mass. This is because of the analytical dependence of the mass outflow rate on other parameters. For example, for EDW of two different velocities having the same $\dot{M}_{BH}$ and $\dot{M}_w$, equating the factor $(2\epsilon_f\epsilon_r c^2/v_w^2)$ in equation (8) gives $\epsilon_{f1}/v_{w1}^2 = \epsilon_{f2}/v_{w2}^2$. Therefore, faster winds ($v_{w2} > v_{w1}$) need higher feedback efficiency ($\epsilon_{f2} > \epsilon_{f1}$), to hold the previous equality. Our simulations explore EDW of $v_{w1} = 5000$ and $v_{w2} = 10\,000\,\mathrm{km\,s^{-1}}$. In order to have the same BH mass, this analytical estimate predicts $\epsilon_{f2} = \epsilon_{f1}(v_{w2}/v_{w1})^2 = 4\epsilon_{f1}$. The best-fitting parameters that we obtain for the isolated galaxy are $\epsilon_{f1} = 0.05$ and $\epsilon_{f2} = 0.25$, whose ratio (5) is very close to the analytical prediction (4).

The slope of the observational $[M_{BH}-\sigma_\star]$ correlation has been revised over the last decade owing to sample selection effects and continuous newer data. Results depend on whether or not barred and/or pseudo-bulge galaxies are included in the analysis, and statistical regression methods used to fit the data. The observations by Tremaine et al. (2002) and Gultekin et al. (2009) based on which we calibrate our model parameters have a $[M_{BH}-\sigma_\star]$ logarithmic slope of $\sim$4. In a relatively recent study McConnell & Ma (2013), using new and revised kinematic data of a larger sample, presented significantly steeper $[M_{BH}-\sigma_\star]$ relation of slope $\sim$5. This steepening has occurred because of newest dynamical measurements of BH mass. Using observations of barred and non-barred galaxies, Graham et al. (2011) and Graham & Scott (2013) also found a steeper $[M_{BH}-\sigma_\star]$ slope of around 5–5.5 for elliptical and unbarred galaxies. Kormendy & Ho (2013) recently reported a slope of 4.4 for $[M_{BH}-\sigma_\star]$, almost mid-way between the values 4 and 5

obtained in other studies. Studying semi-analytical models, Shankar et al. (2012) showed that the scatter in the updated local BH–bulge mass relation appears to be quite large when including late-type galaxies. Sadoun & Colin (2012) inferred observational evidence that the BH mass correlates with the velocity dispersion of globular cluster systems in their host galaxies; the relation having a flatter slope, a higher normalization and less scatter.

We perform one isolated galaxy simulation (*kinE2* case) with 10 times higher resolution (run *hi-res*), to test resolution effects. We find that the *hi-res* results are qualitatively similar to that of *kinE2*, but not technically converged. The SFR depends on the resolved gas density, while BH growth depends on SFR through the local gas properties, because SF depletes gas, reducing that available for BH accretion. Therefore, full convergence cannot be expected with the same parameter values of the subgrid models. The SFR is more in the *hi-res* case, since higher densities are resolved, and the mass of new stars formed is ∼1.5 per cent larger, consequently the BH is five times less massive at 2 Gyr, and less gas mass outflows after 0.7 Gyr. The lack of convergence of the BH mass implies that different model parameters (e.g. ϵ_f, v_w) are required to have the same $[M_{BH}-\sigma_\star]$ fit at different resolution. Here, a rigorous numerical convergence would first require tuning of the SF model parameters. For example, Guedes et al. (2011) found that their SF prescription requires higher density thresholds at increased resolutions. We find that the fluctuating nature of the rapidly varying quantities (BHAR and SFR in Fig. 4) remain the same between *kinE2* and *hi-res* cases.

Our results demonstrate that the current implementation of BH thermal feedback has essentially no effect within the framework of the standard multiphase SF model (Springel & Hernquist 2003), where SF is based on a density threshold only. The thermal energy deposited to the gas particles which are multiphase (star forming) is radiated away instantaneously, since they are dense. And they attain the effective equation-of-state temperature dictated by their density. This process might even induce SF by heating, since increasing the temperature of a multiphase particle makes the cold phase more pressurized. This mimics the positive AGN feedback phenomenon of triggering starbursts by AGN outflows, when they compress clumpy gas clouds (e.g. Natarajan, Sigurdsson & Silk 1998; Mellema, Kurk & Rottgering 2002; Barai & Wiita 2007; Gaibler et al. 2012).

The non-effectiveness of the thermal feedback is aggravated in our models by the hole detection numerical algorithm (Section 2.3.1), first used in this study. The SFR in our simulations is directly proportional to the gas mass inside $2\,h^{-1}$ kpc, implying that SF quenching happens by removal of gas. We extrapolate that all the studies (e.g. Di Matteo et al. 2005) using the BH numerical methodology of Springel et al. (2005) are plagued by such artefacts: those incur a thermal feedback induced SF quenching by gas depletion via the creation of a hole around the BH location, and not actually by heating the gas. However, we limit the expansion of the hole using our novel numerical technique, which restricts the gas depletion, therefore, allows SF to occur unrestricted, bounding the impact of SF reduction.

Note that Booth & Schaye (2009) employed schemes to solve these problems, and the improved BH subgrid model has been used in their subsequent cosmological simulations (e.g. Schaye et al. 2010; van de Voort et al. 2011; Haas et al. 2013). Booth & Schaye (2009) showed analytically that when $\alpha = 100$ is adopted, the BHAR of massive BHs is Eddington limited (i.e. independent of density) down to very low gas density, and drops below Eddington only at even lower densities. They introduced a density-dependent α factor in the Bondi rate, which enables a BH to lower its accretion rate

at higher gas densities, overall reducing the possibility of creating an artificial hole in the gas distribution. Furthermore, Booth & Schaye (2009) made thermal AGN feedback efficient by setting a minimum heating temperature of 10^8 K, and allowing strongly heated gas (even if denser than SF threshold) to leave the effective SF equation of state.

Modifications are needed in the BH thermal feedback subgrid model in order to make it effective. One amendment is to not allow the thermally heated gas to form stars, to ensure the negative nature of AGN feedback. In subgrid models, this amounts to imposing an upper temperature threshold for SF, such that only gas at lower temperatures form stars (e.g. Vogelsberger et al. 2013). An alternative method for BH thermal energy distribution is described in appendix A4 of Ragone-Figueroa et al. (2013). The efficient implementation of thermal SNe feedback in galaxy simulations is a related issue; Dalla Vecchia & Schaye (2012) prescribed a scheme where the gas is heated to a minimum heating temperature and shows strong feedback effects.

The mass of newly formed stars together with the initial disc and bulge stars, plotted in the bottom row of Fig. 2, is indistinguishable between the three runs (*SF*, *th1* and *kinE1*). We checked that at $t = 1.73$ Gyr, the mass of new stars formed is the same for the no BH and thermal feedback cases and 0.8 times smaller in the kinetic feedback model. However, this new star mass ($\sim 3.7 \times 10^9\,M_\odot$) is 12 times smaller than the combined disc and bulge stellar components present in the initial galaxy models ($4.7 \times 10^{10}\,M_\odot$, Table 1). Thus, the total stellar mass is dominated by the old stars of disc and bulge, and the newly formed ones contribute just a small fraction.

The Z_C profiles of the merged galaxy (Fig. 8) reveal that the differences between the models are most prominent in the lower mass and fiducial galaxies (of total masses $M_{tot}/M_\odot = 1.40 \times 10^{11}$ and 1.12×10^{12}), where kinetic feedback results up to (10–1000) times higher Z_C than thermal, within $r \sim (20–100)\,h^{-1}$ kpc. Hence, we infer that the CGM gas at such galactocentric distances can give the best Z_C observational diagnostic to distinguish between various BH feedback models. Other studies also find that kinetic AGN feedback can uplift metals from galaxy to 100s of kpc (e.g. Gaspari et al. 2011a), making metallicity diagnostics an excellent way to differentiate feedback models.

We note the possibility that parts of an outflow might effectively change type between kinetic and thermal. A kinetically driven outflow, which is generally a fast wind, can shock and thermalize along its path in the central regions of the galaxy, and parts of it may turn to a slow thermal outflow. A thermally driven wind, which is hot and isotropic, can evaporate cold clumps, generating fast kinetic wind components. However, signatures of the original distinct feedback mode: isotropic thermal blast versus bipolar kinetic wind, remain different, which we try to diagnose in our study by the different galaxy properties.

Physical processes like fragmentation, instabilities and turbulence are important, occurring on small scales within the galaxy ISM or in the outflows. However, the resolution of our simulations is too low to model these phenomena. The gas particle mass is $1.8 \times 10^5\,M_\odot$ (Table 1) in our fiducial galaxy, and the gravitational softening length is $0.5/h$ kpc. In order to study the effects of instabilities, sub-pc resolution is required. For example, simulations by Barai et al. (2012) (where the gas particle mass is $0.8\,M_\odot$) and Gaspari et al. (2013) found thermal-instability-driven fragmentation. Thus, our too coarse resolution renders it impossible to explore such small-scale processes. Intuitively, in the presence of hydrodynamic instabilities (such as Kelvin–Helmholtz and Rayleigh–Taylor) and/or thermal instability, the outflows would have lower

velocities and higher mass outflow rates by entrainment of more gas. The morphological differences of the various feedback modes would then be somewhat reduced. However, over several Gyr, the BH mass is expected to remain the same via self-regulation.

5 SUMMARY AND CONCLUSION

We investigate different modes of AGN feedback in galaxy simulations. We examine two physical ways in which the feedback energy from a BH is coupled to the neighbouring gas: *thermal* – where the temperature is increased and *kinetic* – where the velocity is boosted. We formulate kinetic feedback models with two free parameters: feedback efficiency and AGN wind velocity. The models are implemented in the TreePM – SPH code GADGET-3: gas particles are stochastically selected from the neighbours and imparted a one-time $v_{\rm w}$ boost. We incorporate a novel numerical algorithm to detect the existence of a hole in the gas distribution around the BH, and prevent its expansion. The code includes additional subresolution physics: metal-dependent radiative cooling and heating, SF, stellar evolution and chemical enrichment.

We perform simulations of isolated and merging disc galaxies, of total mass $1.12 \times 10^{12}\,{\rm M}_\odot$ (similar as the Milky Way) in our fiducial case. Each initial galaxy model contains 3×10^5 DM, 5×10^4 disc gas, 25×10^3 disc star and 25×10^3 bulge star particles. New stars form during the simulation, and in our analysis of $\sigma_\star$ all the stars are counted. The collisionless BH particle has an initial dynamical mass 1.6 times the DM particle mass and a seed mass of $10^5\,{\rm M}_\odot$. For the merger simulations, two equal-mass isolated galaxies are set on a parabolic collision course. We perform runs with the same non-AGN physics, and varying the AGN feedback models:

– SF and chemical enrichment only (no BH),
– thermal BH feedback,
– kinetic BH feedback with EDW prescription, and
– kinetic BH feedback with MDW.

The results are summarized below.

(i) We compare the $M_{\rm BH}$ versus $\sigma_\star$ obtained in our simulations with observational data. All the stars lying within the stellar half-mass radius are tracked, and the median stellar velocity dispersion is estimated from hundred random LOS directions. The parameters giving a best fit in the isolated galaxy are for BH thermal feedback $\epsilon_{\rm f} = 0.01$; for BH kinetic EDW $v_{\rm w} = 5000\,{\rm km\,s^{-1}}$ with $\epsilon_{\rm f} = 0.05$ and $v_{\rm w} = 10\,000\,{\rm km\,s^{-1}}$ with $\epsilon_{\rm f} = 0.25$; for BH kinetic MDW $v_{\rm w} = 2500\,{\rm km\,s^{-1}}$ with $\epsilon_{\rm f} = 1$. We obtain the following best-fitting parameters in the galaxy merger: for BH thermal $\epsilon_{\rm f} = 0.05$; for BH kinetic EDW $v_{\rm w} = 5000$ or $10\,000\,{\rm km\,s^{-1}}$ with $\epsilon_{\rm f} = 0.25$. For BH kinetic MDW feedback, none of the parameters we explored fit the observations; the BH mass is always too large. Our best-fitting model parameters are dependent on simulation resolution, because SFR depends on the resolved gas density, affecting BH growth.

(ii) In the isolated galaxy, there is no gas outflow in the SF only case. BH thermal feedback produces a late weak outflow, with 10^{-3} of all gas ejected after 1 Gyr. BH kinetic feedback produces gas outbursts from 0.2 Gyr, as bipolar jet-like outflows visible intermittently, separated by longer quiescent intervals, with 0.03–0.07 of the gas mass outflown by 1 Gyr. This results in a smaller stellar mass.

(iii) In the merging galaxy pair, collisions, shock heating and tidal interactions cause significant gas outflow from the beginning, even in the SF only case. BH models induce enhanced outflow: in thermal feedback up to two times higher than SF only, and in

kinetic feedback 5–8 times more. The galaxies pass through a first and second pericentres at 0.4 and 1.9 Gyr, and coalesce between (2–2.5) Gyr. The resulting merged galaxy has an extended, diffuse, spheroidal gaseous halo. Stellar and gas distributions are more spherically shaped in the SF only run, irregular to elliptically shaped with kinetic feedback and intermediate with thermal.

(iv) The BH mass growth occurs in a qualitatively similar manner for all the models: slow growth initially, exponential growth from $t \sim 0.5$ Gyr until 1 Gyr in the isolated galaxy and until 1.5 Gyr in the merger when its mass increases by a factor of 10 to a few 100 depending on the AGN model, and an almost steady-state afterward. The final $M_{\rm BH}$ is inversely proportional to $\epsilon_{\rm f}$ and directly to $v_{\rm w}$. The impact of varying $v_{\rm w}$ is reduced in a merger than an isolated galaxy.

(v) The BH mass accretion rate exhibit heavy fluctuations, by a factor of up to 100 in the isolated and 1000 in the merger within 0.02 Gyr.

(vi) The models display similar SFR in the isolated galaxy: at $t > 0.9$ Gyr kinetic feedback generates a 1.5 times lower SFR than the SF only and thermal cases. In the merger, thermal feedback produces a (1.5–10) times lower SFR than the SF only run at $t > 2$ Gyr. Kinetic feedback causes a greater suppression, starting from $t > 1$ Gyr, 5–100 times lower SFR than the SF only case.

We see that the SFR is directly proportional to the gas mass inside $2\,h^{-1}$ kpc, implying that SF quenching happens by removal of gas, and there is very little effect of feedback by gas heating on SFR.

(vii) The temperature radial profiles of the merged galaxy display a local peak in the outer regions, which for the SF only and thermal feedback occurs at a radius 10 times smaller than the kinetic feedback models. Gas density and carbon metallicity profiles demonstrate that kinetic feedback expels dense metal-rich gas out from central regions of galaxies, and enrich the lower density CGM and IGM to >100 kpc. Radial $Z_{\rm C}$ profiles present most prominent differences between the models in galaxies of total masses 1.40×10^{11} and $1.12 \times 10^{12}\,{\rm M}_\odot$: kinetic feedback results up to (10–1000) times higher $Z_{\rm C}$ than thermal, within $r \sim (20$–$100)\,h^{-1}$ kpc; the CGM gas at such galactocentric distances can give the best $Z_{\rm C}$ observational diagnostic to distinguish between BH feedback models.

(viii) The low to negligible impact of BH thermal feedback on gas properties reveal that our adopted methodology from Springel et al. (2005) is ineffective within the framework of the multiphase SF model. It is enhanced by the fact that we limit the expansion of the hole using our novel numerical technique, which restricts gas depletion around the BH. Previous studies using the same BH thermal feedback model had SF quenching by gas depletion via the creation of an artificial hole, and not actually by heating the gas.

We are performing ongoing work to improve the subgrid model of BH thermal feedback, by modifying the way in which feedback energy is distributed and changing the conditions of SF. In the future, we plan to perform cosmological hydrodynamic simulations including unified models of AGN feedback: quasar mode and radio mode (numerically implemented as thermal and kinetic feedback from BH), to study BH–galaxy coevolution and IGM properties.

REFERENCES

Asplund M., Grevesse N., Sauval A. J., 2005, ASP Conf. Ser. Vol. 336, Cosmic Abundances as Records of Stellar Evolution and Nucleosynthesis. Astron. Soc. Pac., San Francisco, p. 25

Barai P., 2008, ApJ, 682, L17

Barai P., Wiita P. J., 2006, MNRAS, 372, 381

Barai P., Wiita P. J., 2007, ApJ, 658, 217

Barai P., Proga D., Nagamine K., 2011a, MNRAS, 418, 591

Barai P., Martel H., Germain J., 2011b, ApJ, 727, 54

Barai P., Proga D., Nagamine K., 2012, MNRAS, 424, 728

Barai P. et al., 2013, MNRAS, 430, 3213

Begelman M. C., Nath B. B., 2005, MNRAS, 361, 1387

Bondi H., 1952, MNRAS, 112, 195

Bondi H., Hoyle F., 1944, MNRAS, 104, 273

Booth C. M., Schaye J., 2009, MNRAS, 398, 53

Chabrier G., 2003, PASP, 115, 763

Chambers K. C., Miley G. K., van Breugel W., 1987, Nat, 329, 604

Crenshaw D. M., Kraemer S. B., George I. M., 2003, ARA&A, 41, 117

Croton D. J. et al., 2006, MNRAS, 365, 11

Dalla Vecchia C., Schaye J., 2012, MNRAS, 426, 140

De Young D. S., 1989, ApJ, 342, L59

Debuhr J., Quataert E., Ma C.-P., Hopkins P., 2010, MNRAS, 406, L55

Debuhr J., Quataert E., Ma C.-P., 2011, MNRAS, 412, 1341

Debuhr J., Quataert E., Ma C.-P., 2012, MNRAS, 420, 2221

Di Matteo T., Springel V., Hernquist L., 2005, Nat, 433, 604

Di Matteo T., Colberg J., Springel V., Hernquist L., Sijacki D., 2008, ApJ, 676, 33

Di Matteo T., Khandai N., DeGraf C., Feng Y., Croft R. A. C., Lopez J., Springel V., 2012, ApJ, 745, L29

Dubois Y., Devriendt J., Slyz A., Teyssier R., 2010, MNRAS, 409, 985

Dubois Y., Pichon C., Devriendt J., Silk J., Haehnelt M., Kimm T., Slyz A., 2013a, MNRAS, 428, 2885

Dubois Y., Gavazzi R., Peirani S., Silk J., 2013b, MNRAS, MNRAS, 433, 3297

Everett J. E., 2007, Ap&SS, 311, 269

Fabian A. C., 2012, ARA&A, 50, 455

Fabjan D., Borgani S., Tornatore L., Saro A., Murante G., Dolag K., 2010, MNRAS, 401, 1670

Ferrarese L., Ford H., 2005, Space Sci. Rev., 116, 523

Feruglio C., Maiolino R., Piconcelli E., Menci N., Aussel H., Lamastra A., Fiore F., 2010, A&A, 518, L155

Gabor J. M., Bournaud F., 2013, MNRAS, 434, 606

Gaibler V., Khochfar S., Krause M., Silk J., 2012, MNRAS, 425, 438

Gaspari M., Melioli C., Brighenti F., D'Ercole A., 2011a, MNRAS, 411, 349

Gaspari M., Brighenti F., D'Ercole A., Melioli C., 2011b, MNRAS, 415, 1549

Gaspari M., Brighenti F., Temi P., 2012a, MNRAS, 424, 190

Gaspari M., Ruszkowski M., Sharma P., 2012b, ApJ, 746, 94

Gaspari M., Ruszkowski M., Oh S. P., 2013, MNRAS, 432, 3401

Gebhardt K. et al., 2000, ApJ, 539, L13

Germain J., Barai P., Martel H., 2009, ApJ, 704, 1002

Graham A. W., Scott N., 2013, ApJ, 764, 151

Graham A. W., Onken C. A., Athanassoula E., Combes F., 2011, MNRAS, 412, 2211

Granato G. L., De Zotti G., Silva L., Bressan A., Danese L., 2004, ApJ, 600, 580

Guedes J., Callegari S., Madau P., Mayer L., 2011, ApJ, 742, 76

Gultekin K. et al., 2009, ApJ, 698, 198

Haardt F., Madau P., 2001, in Neumann D. M., Van J. T. T., eds, XXIst Moriond Astrophysics Meeting. Editions Frontières, Gif-sur-Yvette, p. 64

Haas M. R., Schaye J., Booth C. M., Dalla Vecchia C., Springel V., Theuns T., Wiersma R. P. C., 2013, MNRAS, 435, 2931

Hernquist L., 1990, ApJ, 356, 359

Hirschmann M., Dolag K., Saro A., Borgani S., Burkert A., 2013, preprint (arXiv:1308.0333)

Hobbs A., Power C., Nayakshin S., King A. R., 2012, MNRAS, 421, 3443

Hoyle F., Lyttleton R. A., 1939, Proc. Camb. Phil. Soc., 35, 405

Johansson P. H., Naab T., Burkert A., 2009a, ApJ, 690, 802

Johansson P. H., Burkert A., Naab T., 2009b, ApJ, 707, L184

Katz N., Weinberg D. H., Hernquist L., 1996, ApJS, 105, 19

Khalatyan A., Cattaneo A., Schramm M., Gottlober S., Steinmetz M., Wisotzki L., 2008, MNRAS, 387, 13

King A., 2003, ApJ, 596, L27

Komatsu E. et al., 2011, ApJS, 192, 18

Kormendy J., Ho L. C., 2013, ARA&A, 51, 511

Kormendy J., Richstone D., 1995, ARA&A, 33, 581

Krongold Y., Nicastro F., Elvis M., Brickhouse N., Binette L., Mathur S., Jimenez-Bailon E., 2007, ApJ, 659, 1022

Magorrian J. et al., 1998, AJ, 115, 2285

Maio U., Dotti M., Petkova M., Perego A., Volonteri M., 2013, ApJ, 767, 37

McConnell N. J., Ma C.-P., 2013, ApJ, 764, 184

Mellema G., Kurk J. D., Rottgering H. J. A., 2002, A&A, 395, L13

Natarajan P., Sigurdsson S., Silk J., 1998, MNRAS, 298, 577

Nesvadba N. P. H., Lehnert M. D., De Breuck C., Gilbert A. M., van Breugel W., 2008, A&A, 491, 407

Newton R. D. A., Kay S. T., 2013, MNRAS, 434, 3606

Okamoto T., Nemmen R. S., Bower R. G., 2008, MNRAS, 385, 161

Ostriker J. P., Choi E., Ciotti L., Novak G. S., Proga D., 2010, ApJ, 722, 642

Padovani P., Matteucci F., 1993, ApJ, 416, 26

Power C., Nayakshin S., King A., 2011, MNRAS, 412, 269

Ragone-Figueroa C., Granato G. L., Murante G., Borgani S., Cui W., 2013, MNRAS, preprint (arXiv:1308.3246)

Reichard T. A. et al., 2003, AJ, 126, 2594

Rupke D. S. N., Veilleux S., 2011, ApJ, 729, L27

Sadoun R., Colin J., 2012, MNRAS, 426, L51

Salucci P., Szuszkiewicz E., Monaco P., Danese L., 1999, MNRAS, 307, 637

Scannapieco E., Silk J., Bouwens R., 2005, ApJ, 635, L13

Schawinski K. et al., 2006, Nat, 442, 888

Schaye J. et al., 2010, MNRAS, 402, 1536

Shakura N. I., Sunyaev R. A., 1973, A&A, 24, 337

Shankar F., Salucci P., Granato G. L., De Zotti G., Danese L., 2004, MNRAS, 354, 1020

Shankar F., Lapi A., Salucci P., De Zotti G., Danese L., 2006, ApJ, 643, 14

Shankar F., Marulli F., Mathur S., Bernardi M., Bournaud F., 2012, A&A, 540, A23

Sijacki D., Springel V., Di Matteo T., Hernquist L., 2007, MNRAS, 380, 877

Sijacki D., Springel V., Haehnelt M. G., 2009, MNRAS, 400, 100

Silk J., 2005, MNRAS, 364, 1337

Silk J., Rees M. J., 1998, A&A, 331, L1

Springel V., 2005, MNRAS, 364, 1105

Springel V., Hernquist L., 2003, MNRAS, 339, 289

Springel V., White S. D. M., 1999, MNRAS, 307, 162

Springel V., Di Matteo T., Hernquist L., 2005, MNRAS, 361, 776

Sturm E. et al., 2011, ApJ, 733, L16

Tescari E., Viel M., Tornatore L., Borgani S., 2009, MNRAS, 397, 411

Tescari E., Viel M., D'Odorico V., Cristiani S., Calura F., Borgani S., Tornatore L., 2011, MNRAS, 411, 826

Thielemann F.-K. et al., 2003, Nucl. Phys. A, 718, 139

Tombesi F., Cappi M., Reeves J. N., Nemmen R. S., Braito V., Gaspari M., Reynolds C. S., 2013, MNRAS, 430, 1102

Tornatore L., Borgani S., Dolag K., Matteucci F., 2007, MNRAS, 382, 1050

Tremaine S. et al., 2002, ApJ, 574, 740

van de Voort F., Schaye J., Booth C. M., Dalla Vecchia C., 2011, MNRAS, 415, 2782

van den Hoek L. B., Groenewegen M. A. T., 1997, A&AS, 123, 305

Vazza F., Bruggen M., Gheller C., 2013, MNRAS, 428, 2366

Vogelsberger M., Genel S., Sijacki D., Torrey P., Springel V., Hernquist L., 2013, preprint (arXiv:1305.2913)

Wagner A. Y., Umemura M., Bicknell G. V., 2013, ApJ, 763, L18

Wang J.-M., Chen Y.-M., Yan C.-S., Hu C., Bian W.-H., 2007, ApJ, 661, L143

Wiersma R. P. C., Schaye J., Smith B. D., 2009, MNRAS, 393, 99

Woosley S. E., Weaver T. A., 1995, ApJS, 101, 181

Wurster J., Thacker R. J., 2013a, MNRAS, 431, 539

Wurster J., Thacker R. J., 2013b, MNRAS, 431, 2513

Zinn P.-C., Middelberg E., Norris R. P., Dettmar R.-J., 2013, ApJ, 774, 66

Zubovas K., Nayakshin S., King A., Wilkinson M., 2013, MNRAS, 433, 3079

This paper has been typeset from a TEX/LATEX file prepared by the author.